Journal of Geophysical Research: Solid Earth

RESEARCH ARTICLE
10.1002/2017JB014928

Key Points:
- The CE 1303 Hongdong earthquake was a dip-slip extensional event on the Huoshan Piedmont Fault
- The CE 1303 earthquake had a magnitude in the range M_w 7.2–7.6
- Ordos earthquakes are not exceptions to the global pattern of normal fault events with $M < 8$ as the upper limit

Supporting Information:
- Supporting Information S1

Correspondence to:
H. He,
honglinhe123@vip.sina.com

Citation:
Xu, Y., He, H., Deng, Q., Allen, M. B., Sun, H., & Bi, L. (2018). The CE 1303 Hongdong earthquake and the Huoshan Piedmont Fault, Shanxi Graben: Implications for magnitude limits of normal fault earthquakes. *Journal of Geophysical Research: Solid Earth*, *123*, 3098–3121. https://doi.org/10.1002/2017JB014928

Received 2 SEP 2017
Accepted 14 MAR 2018
Accepted article online 23 MAR 2018
Published online 22 APR 2018

The CE 1303 Hongdong Earthquake and the Huoshan Piedmont Fault, Shanxi Graben: Implications for Magnitude Limits of Normal Fault Earthquakes

Yueren Xu[1,2,3], Honglin He[1], Qidong Deng[1], Mark B. Allen[3], Haoyue Sun[1], and Lisi Bi[4]

[1]Key Laboratory of Active Tectonics and Volcano, Institute of Geology, China Earthquake Administration, Beijing, China, [2]Key Laboratory of Earthquake Predication, Institute of Earthquake Forecasting, China Earthquake Administration, Beijing, China, [3]Department of Earth Sciences, University of Durham, Durham, UK, [4]Key Laboratory of Earthquake Monitoring and Disaster Mitigation Technology, Earthquake Administration of Guangdong Province, Guangzhou, China

Abstract The CE 1303 Hongdong earthquake, with ~270,000 deaths, has been suggested as the first magnitude 8 earthquake recorded in North China. We use 31 AMS-14C ages to date earthquakes recorded in the Huoshan Piedmont Fault, which is interpreted to be the causative fault for the event. We interpret fault traces and map the Hongdong earthquake surface rupture in detail. Four events are identified with timings constrained at 1,060–590 year BP (corresponding to the Common Era 1303 event), 3,310–3,210 year BP, 5,460–5,380 year BP, and 26,380 year BP, respectively. The later three events have a recurrence interval of ~2,000–3,000 years. We find that the Hongdong earthquake had a rupture length of ~98 km, a maximum throw of 5.0 m and a best estimate for magnitude in the range Mw 7.2–7.6. We suggest that previous magnitude estimates are overestimates. Normal fault earthquakes have smaller upper limits to their magnitudes than thrusts, because their relatively steep dips produce intersections at the base of the seismogenic layer at smaller downdip widths than gently dipping thrust faults. The Hongdong event was not an exception to this pattern. The historic released seismic moment may be closer to the accumulated moment than previously calculated.

Plain Language Summary The Common Era 1303 Hongdong earthquake with ~270,000 deaths suggested as the first *M* 8 in North China. We use 31 AMS-^{14}C ages to date earthquakes recorded in the Huoshan Piedmont Fault, which is interpreted to be the causative fault for the event. We interpret fault traces and map the Hongdong earthquake rupture in detail. Four events are identified with timings constrained at 1,060–590 year BP (corresponding to the Common Era 1303 event), 3,310–3,210 year BP, 5,460–5,380 year BP, and 26,380 year BP, respectively. The later three events have a recurrence interval of ~2,000–3,000 years. We find that the earthquake had a rupture length of ~98 km, and a maximum throw of 5.0 m, and a best estimate for magnitude in the range M_w 7.2–7.6. We suggest that previous magnitude estimates are overestimates. Normal fault earthquakes have smaller upper limits to their magnitudes than thrusts, because their relatively steep dips produce intersections at the base of the seismogenic layer at smaller downdip widths than gently dipping thrust faults. The Hongdong event was not an exception to this pattern. The historic released seismic moment may be closer to the accumulated moment than previously calculated.

1. Introduction

This paper is a study of the Common Era (CE) 1303 Hongdong earthquake, located on the eastern side of the Ordos Plateau, North China (Figure 1), in which ~270,000 people were reportedly killed (Meng & Lin, 1972; Qi, 1983, 2005; Yao et al., 1984). We assess the Hongdong earthquake through a paleoseismicity study and evaluate whether or not it was in the *M* 8 range (Geophysical Institute of Academy of Science of China (GIASC) et al., 2003; State Seismological Bureau (SSB), 1988), with implications for processes of extensional deformation in the continents. If the *M* ~ 8 magnitude is confirmed, it would be one of the largest normal fault earthquakes on record. If it was *M* ~ 7, it would reinforce the distinction in maximum magnitude between normal fault earthquakes and other types of event, with implications for continental tectonic processes (Middleton et al., 2016). Our paleoseismicity study also reveals older ruptures along the Huoshan Piedmont Fault (HPF), such that we can provide a constraint on the recurrence interval for major earthquakes on this structure.

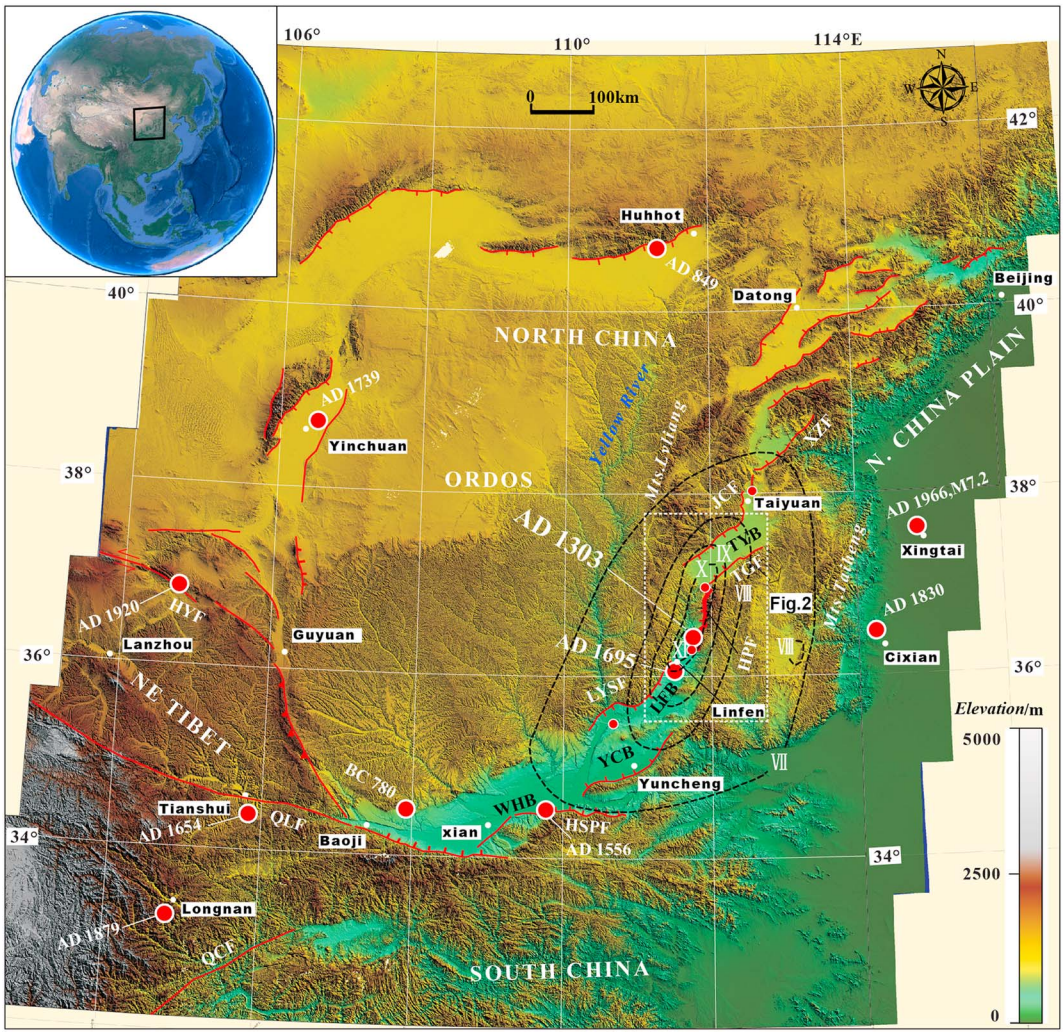

Figure 1. Shuttle Radar Topography Mission topography of the Ordos Plateau in North China. The red lines are major active faults. The red circles are major historical and modern earthquakes (State Seismological Bureau (SSB), 1988; Working Group on Historical Earthquake Compilation of Shanxi Province Earthquake Administration (WGHECSPEA), 1991) with magnitudes >4.6. The black dashed lines are isoseismals for the CE 1303 Hongdong earthquake according to the new Chinese intensity scale (Shanxi Province Institute of Earthquake Engineering Investigation (SPIEEI), 2009). Inset globe shows the location of Figure 1 within Asia. Major faulted basins: TYB, Taiyuan Basin; LFB, Linfen Basin; YCB, Yuncheng Basin; WHB, Weihe Basin; JCF, Jiaocheng Fault; TGF, Taigu Fault; LYSF, Luoyuoshan Fault; HPF, Huoshan Piedmont Fault; QCF, Qingchuan Fault; QLF, Qinling Fault; HSPF, Huoshan Piedmont Fault.

Normal-faulting earthquakes in North China occur in a slowly extending region. The extension rate across the Shanxi Graben System (Figures 1 and 2) is modest, at 0.8 ± 0.3 mm/year (Wang et al., 2011; Zhang & Gan, 2008), so that recurrence intervals are long; there has been no major ($M \geq 7$) earthquake in the Shanxi Graben System during the instrumental period. Although these events are comparatively infrequent, their large sizes mean that they pose a significant seismic risk to densely populated areas of Shanxi, Shaanxi, Gansu, and neighboring provinces (Middleton et al., 2016). Taiyuan and Linfen cities now have populations of >3 million and ~1 million, respectively (Figure 2), and a similarly large earthquake will lead to even more destruction than in CE 1303.

Published magnitudes of these North China earthquakes may be inaccurate, given that estimates are largely based on descriptions in historical records, and emphasize the importance of high death tolls rather than direct physical parameters. Additionally, magnitude estimates based partly on shaking intensities have to be treated with caution. Many parts of the Ordos region are underlain by loess deposits or by loess reworked into fluvial and/or lacustrine sediments deposited by the Yellow River and its tributaries. Such sediments amplify seismic waves. Many researchers have assumed that the magnitude of the

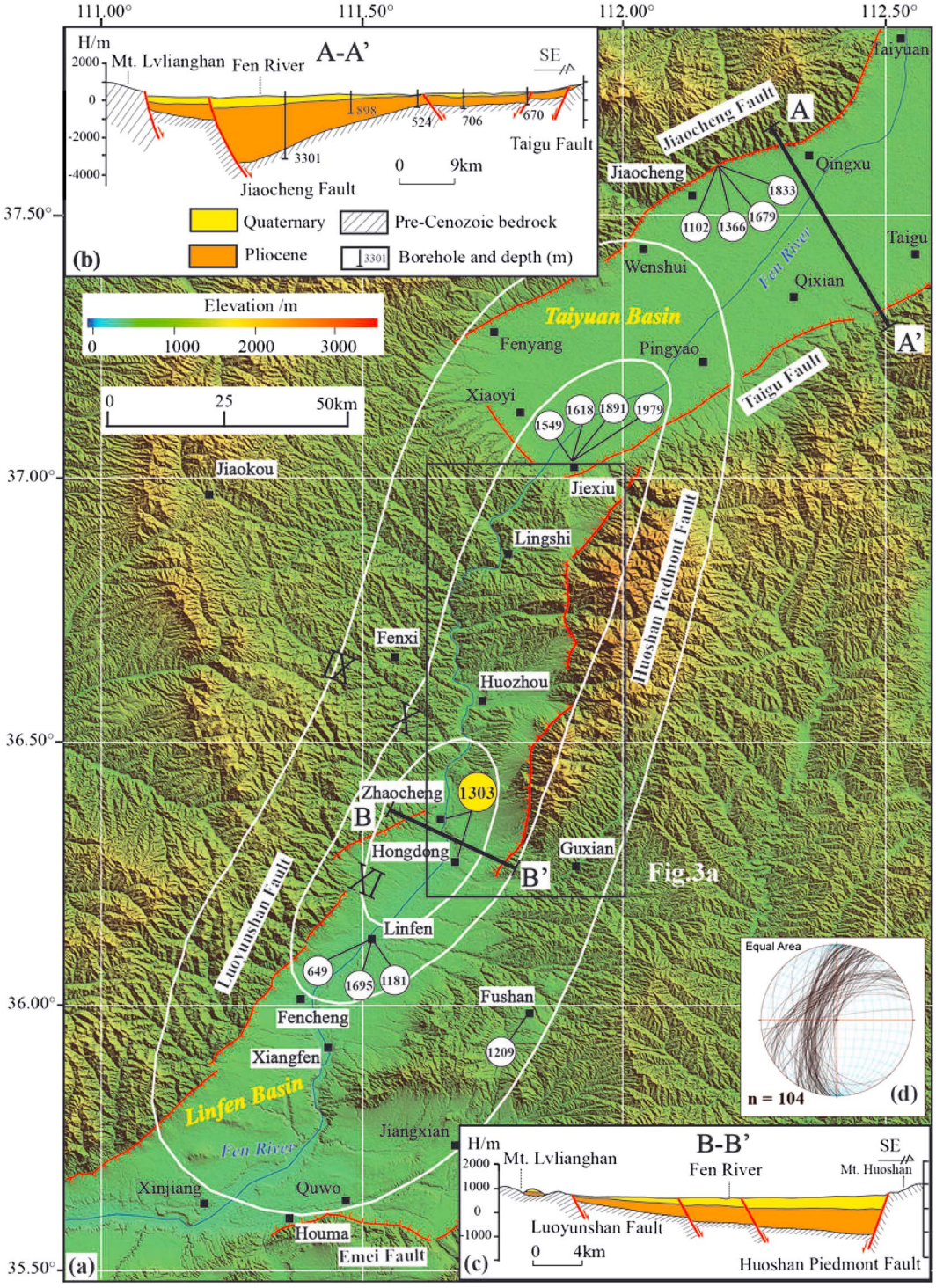

Figure 2. (a) Shuttle Radar Topography Mission topography of the Linfen Basin and southern Taiyuan Basin. Faults (red lines) are mapped from satellite imagery (http://earth.google.com) and Xu, Xie, and Sun (2011), Xu (2013), and Jing et al. (2016). Historical earthquakes (Working Group on Historical Earthquake Compilation of Shanxi Province Earthquake Administration (WGHECSPEA), 1991) are shown by circles, including the year in which they occurred. The white lines show the isoseismals for the CE 1303 earthquake, according to the new Chinese intensity scale (Shanxi Province Institute of Earthquake Engineering Investigation (SPIEEI), 2009). The thick black lines show approximate location of profiles in Figures 2b, 2c. (b) Sketch cross section across the southern Taiyuan Basin based on seismic reflection data and figures in State Seismological Bureau (SSB) (1988) and Xu and Ma (1992). (c) Sketch cross section across the northern Linfen Basin based on Xu et al. (1993). (d) Equal area stereo projection plot of fault plane orientations of the Huoshan Piedmont Fault.

Hongdong earthquake is well constrained and used the accepted $M \sim 8$ value without further analysis (Jiang et al., 2004; Meng, Yu, & Xi, 1985; Shanxi Province Institute of Earthquake Engineering Investigation (SPIEEI), 2009; Shen et al., 2004; State Seismological Bureau (SSB), 1988; Wang et al., 2011; Wesnousky et al., 1984; Working Group on Historical Earthquake Compilation of Shanxi Province Earthquake Administration (WGHECSPEA), 1991; Xie et al., 2004; Xu & Deng, 1990; Xu & Ma, 1992; Xu et al., 1993; Yao et al., 1984). A similar situation has recently been explored for the CE 1739 Yinchuan earthquake, where Middleton et al. (2016) reevaluated M_w as 7.1–7.6, where previous estimates had $M \sim 8$ (State Seismological Bureau (SSB), 1988).

We have excavated and documented five trenches on the southern segment of the Huoshan HPF (Figure 3a), showing the recent faulting of the HPF, including the CE 1303 Hongdong earthquake. 31 AMS-^{14}C ages have been used to date organic material from the trenches, to constrain the ages of paleoearthquakes, recorded by offset sediments. High-resolution satellite imagery has been used to verify the fault trace and map the Hongdong earthquake rupture in detail. We use published scaling relationships to assess the earthquake magnitude. Through this work, we aim to improve understanding of the earthquake record, seismic risk, and regional tectonics of the Shanxi Graben and the wider Ordos region.

2. Geological Setting

2.1. Active Strain in the Central Shanxi Graben System

The Shanxi Graben System has dimensions of 60 by 1,200 km. It lies within Shanxi and adjacent provinces, east of the stable area known as the Ordos plateau (Figure 1). The graben basins are bounded by north-south or northeast-southwest trending normal faults. The central region consists of the Linfen and Taiyuan basins (Figures 1 and 2) (Li et al., 1998; Ma, 1993; Xu & Ma, 1992; Xu et al., 1993; Wang et al., 1996; Zhang et al., 1998).

The Shanxi Graben System is an intraplate rift zone (State Seismological Bureau (SSB), 1988; Xu & Ma, 1992). Extension may have started during the Miocene (Deng et al., 1973, 1999; Chang et al., 2011; Peltzer et al., 1985; Ren et al., 2002; State Seismological Bureau (SSB), 1988; Zhang et al., 1998; Zhu et al., 1999); it has formed mainly since the Pliocene (State Seismological Bureau (SSB), 1988; Xu & Ma, 1992). Wesnousky et al. (1984) estimated a combined north-south right-lateral slip and extension rate of 0.5–1.0 mm/year, suggesting right-lateral slip predominates over extension. This is similar to the 0.5 mm/year extension rate averaged over the Late Pliocene-Quaternary across the central Shanxi Graben (Zhang et al., 1998, 2003). Wang et al. (2011) obtained an extension rate of 0.8 ± 0.3 mm/year and also a right-lateral slip rate of 0.6 ± 0.5 mm/year from Global Positioning System (GPS) data compiled in Zhang and Gan (2008). Field investigations of active faults yielded extension rates of 0.3–0.5 mm/year (Ma, 1993; State Seismological Bureau (SSB), 1988).

As well as the CE 1303 earthquake, other historical earthquakes have been documented in both basins (Figure 2 and Table 1) (Working Group on Historical Earthquake Compilation of Shanxi Province Earthquake Administration (WGHECSPEA), 1991). In particular, three events with numerous deaths occurred in CE 649, CE 1209, and CE 1695. Epicenters are reported at the locations of Linfen and Fushan cities, but this probably relates to the low spatial resolution of original descriptions, rather than a real coincidence.

2.2. Structure of the Linfen and Taiyuan Basins

The Taiyuan Basin is controlled by the Jiaocheng Fault on the northwestern margin and the Taigu Fault on the southeast margin (Figure 2b). The thickness of sediments in the Taiyuan Basin reaches a maximum of ~3,800 m near the Jiaocheng Fault (State Seismological Bureau (SSB), 1988; Xu et al., 1993). The structure of Linfen Basin is similarly asymmetrical (Figure 2c); the main depocenter (2,200 m thickness) lies near the western side of the basin, controlled by the Luoyunshan Fault (Li, Liu, et al., 2014; State Seismological Bureau (SSB), 1988; Xu, 2013; Xu & Ma, 1992). However, the sedimentary depocenter in the northern part lies near the eastern margin and is controlled by the HPF, with a sediment thickness of 1,600 m (Figure 2c). Mountainous regions at the basin margins consist of Archean gneiss and Paleozoic and Mesozoic strata (Shanxi Provincial Geological Exploration Bureau (SPGEB), 1975).

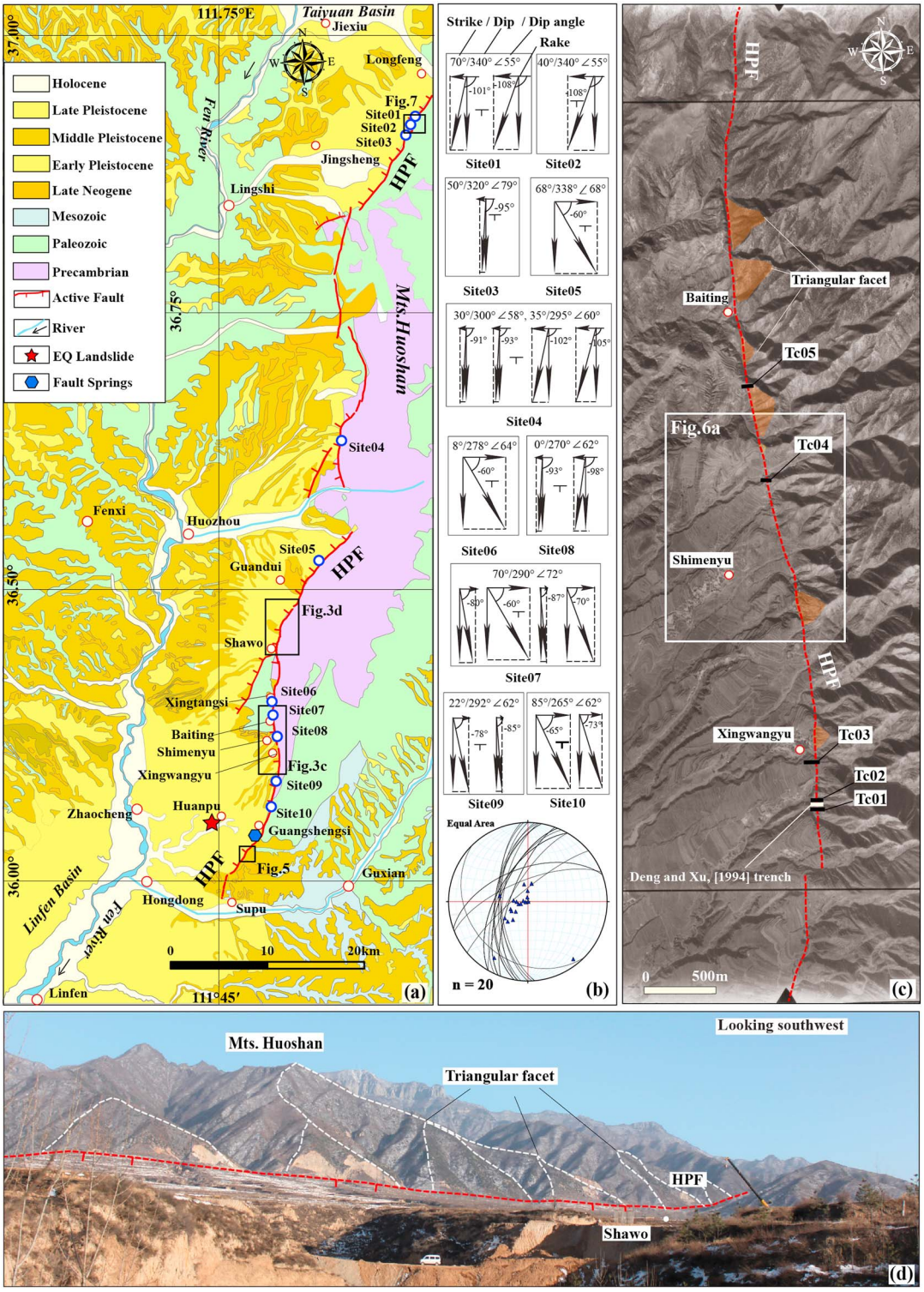

Figure 3. (a) Tectonic outline of the study area. The red lines mark normal faults. Stratigraphic data from Shanxi Provincial Geological Exploration Bureau (SPGEB) (1975) and fieldwork. (b) 20 fault striation data in equal area stereo projection from 10 fault plane segments of the Huoshan Piedmont Fault (locations in Figure 3a) XX°/XX°∠XX° shows strike, dip direction, and dip angle of each fault profile, respectively. The thick main vectors show the slip along the fault plane, the horizontal arrows show the horizontal component, and the vertical arrows show the dip-slip component; i.e., the value of −72° in site 2 shows the rake. The great circles show fault planes, and the blue triangles show the striation rake. (c) Locations of the five trenches in this study. Background is an aerial photograph. The orange triangles are triangular facets. The red lines indicate faults. (d) Photograph of the Huoshan Piedmont Fault at the boundary of Mount Huoshan, with alluvial fans and triangular facets along the fault trace.

Table 1
Historical Earthquakes in the Northern Linfen Basin and Southern Taiyuan Basin[a]

Dates of earthquakes (CE)	Descriptions	Significance of the earthquake
15 Sep 649	Felt across a large area including Linfen, Yuncheng (~125 km southwest of Linfen), especially serious in Linfen, houses destroyed, ~5,000 people killed. 7 aftershocks.	Epicenter near Linfen.
23 Feb 1181	Felt across a large area including Yuncheng, Linfen, and Qinyang (~167 km southeast of Linfen), city wall destroyed, people and animal killed. Aftershocks occurred over 10 days.	Epicenter uncertain.
11 Dec 1209	Earthquake in Linfen Basin, especially serious in Fushan (~31 km east of Linfen), 70–80% houses destroyed, 2,000–3,000 people killed.	Epicenter near Fushan.
01 Sep 1291	Earthquake in Linfen, 10,826 houses destroyed, 150 people killed.	Epicenter near Linfen.
25 Sep 1303	**Earthquake in Taiyuan and Linfen, ~270,000 people killed. Government relief.** In Taiyuan Basin, the ground cracked and springs emerged in Qingxu, Qixian, Pingyao (3,636 people killed), Jiexiu, Fenyang, and Xiaoyi in southern Taiyuan Basin. In Linfen Basin, length of the giant landslides is up to 5 km.Between the two basins, temples all destroyed in Huozhou, and mountain collapses and temples destroyed in Fenxi.	Marco-epicenter: between Hongdong and Zhaocheng (Shanxi Province Institute of Earthquake Engineering Investigation (SPIEEI), 2009)
12 Oct 1303	Earthquake in Taiyuan and Linfen.	Aftershock, epicenter uncertain
14 Feb 1304	**Earthquake in Linfen, repaired houses after mainshock destroyed again**	Aftershock, epicenter uncertain
12 Jun 1304	Earthquake in Fenyang	Aftershock, epicenter near Fenyang
11 Sep 1304	Earthquake in Taigu, spring emerged, many people killed.	Aftershock, epicenter near Taigu
02 Apr 1305	**Earthquake in Taiyuan and Linfen, government relief.**	Aftershock, epicenter uncertain
18 Jun 1305	**Earthquake in Taiyuan and Linfen**, leading to changes to two government place names to pray for respite from earthquakes, **government relief.**	Aftershock, epicenter uncertain
01 Jul 1305	Earthquake in Taigu.	Aftershock, epicenter near Taigu
22 Feb 1306	Earthquake in Taiyuan and Linfen, earthquakes frequently occurred.	Aftershock, epicenter uncertain
08 Apr 1549	Earthquake in Jiexiu, much housing destroyed.	Epicenter near Jiexiu
22 Jun 1618	Earthquake in Jiexiu, city walls and housing destroyed, some people killed.	Epicenter near Jiexiu
18 May 1695	Felt in Linfen Basin, particularly serious in Linfen, Hongdong, Fushan, Xiangling (now part of Xiangfen). ~52,600 people killed.	**Epicenter near Linfen**
17 Apr 1891	Earthquake in Jiexiu, Xiaoyi, Fenyang and Pingyao etc.City walls destroyed, ~100 people killed.	Epicenter near Jiexiu
19 Jun 1979	Earthquake in JiexiuSome housing cracks, small-level loess landslides.	Epicenter of 37.02°N, 112.03°E. *M* 5.2. in Jiexiu

[a]See locations of most towns in Figures 2 and 3. Major earthquakes and its aftershocks that may correlate with surface-faulting events on northern Linfen Basin and southern Taiyuan Basin are shown in bold and discussed further in the text. *Data sources*: Working Group on Historical Earthquake Compilation of Shanxi Province Earthquake Administration (WGHECSPEA) (1991), Wang (2003).

2.3. Background to the CE 1303 Hongdong Earthquake

One of the most deadly earthquakes to strike China took place on 25 September CE 1303 at about 12:00 UTC and is referred to as the Hongdong earthquake. It is the oldest magnitude 8.0 event, based on contemporary Chinese documents, which identified the area between Zhaocheng and Hongdong as the epicenter (Meng & Lin, 1972; Shen et al., 2004). Ground shaking in the northern Linfen Basin, southern Taiyuan Basin, and the area between them reached intensity *XI* on the new Chinese intensity scale (Figures 1 and 2) (Shanxi Province Institute of Earthquake Engineering Investigation (SPIEEI), 2009). Further aftershocks were recorded for the next four years after the main shock (Working Group on Historical Earthquake Compilation of Shanxi Province Earthquake Administration (WGHECSPEA), 1991) (see Table 1). Eight main aftershocks were recorded. The total death toll was at least 270,000, which was ~28% of the total population of the affected region (0.97 million) (Meng & Lin, 1972; Qi, 2005). For comparison the modern population of the same area is 11.74 million. In the northern Linfen Basin, there are no buildings predating CE 1303, while in the southern Taiyuan Basin, there are no surviving temples or pagodas south of Pingyao (3,636 people killed), which predate CE 1303 (Table 1) (Meng & Lin, 1972; Wang, 2003). In the area between the two basins, bedrock collapses and landslides were recorded in Fenxi during the event (Figure 2) (Meng & Lin, 1972; Qi, 2005). "House caves" (Yaodong), built into loess hillsides, commonly collapsed.

During the 1950s–1960s, steles and literature related to the Hongdong earthquake were discovered along the Fen river between the southern Taiyuan Basin and the northern Linfen Basin (Geophysical Institute of

Academy of Science of China (GIASC) et al., 2003; Meng & Lin, 1972). Meng et al. (1985) discovered fault planes, landslides, and sand liquefaction features along the HPF. Xu and Deng (1990) documented a 45 km of surface rupture zone caused by the CE 1303 event, along the southern part of the fault zone, with coseismic dextral dislocation of 4–8.6 m and vertical throw of ~3.5–5.0 m (with maximum values measured near Xingwangyu; Figure 3a). They also suggested that the recurrence interval of earthquakes on the HPF is ~1,500–2,000 year (Deng & Xu, 1994; Xu et al., 1993).

Some researchers interpret the HPF as a dextral strike-slip fault, based on evidence for offset stream gullies along its southern segment (Hu et al., 2010; Xu & Deng, 1990; Zhang et al., 1998). However, the latest 1:50,000 mapping survey work shows features more consistent with normal sense slip, including triangular facets and dip-slip fault striations (Figures 2d and 3c) (State Seismological Bureau (SSB), 1988; Xu et al., 2013; Xu, 2013). There is also the issue of the rupture length, which is relevant to the magnitude of the earthquake. Previous estimates have ranged from 45 to 160 km, the higher estimate involving the Taigu Fault (Jiang et al., 2004; Xie et al., 2004; Xu & Deng, 1990).

3. Methods

3.1. Remote Sensing Interpretation of Fault Traces

We collected aerial photography, produced during the 1960s at scales of 1:14,000–1:41,000. We also used high-resolution (1–3 m) satellite imagery such as GF-1, GF-2, SPOT-5, and Google Earth images, which were produced during 2000–2016. We used the imagery to interpret features associated with the HPF, such as the fault scarp, alluvial fans, and triangular facets (Figure 3). River terraces that crossed the fault, and were offset by faulting to form linear scarps, were used to confirm the fault location. We also used a stereo pair of IRS-P5 (2.5 m) images (Bi et al., 2011) to extract a 3-m digital elevation model (Figure 4a), to help us to verify the fault scarp and possible surface traces. Further images are shown in Figures S1–S6.

3.2. Field Observation and Trenching Analysis

On the basis of previous interpretations, we investigated and identified fault scarps and fault planes along the HPF in the field. Differential GPS and a laser distance sensor were used to measure fault parameters such as scarp heights and fault dips.

To better assess the seismic hazard along the HPF, and to investigate the frequency of large earthquakes on this fault, we conducted paleoseimic investigations in the southern segment of the fault (Figure 3c), following the previous interpretation of a recent scarp in this area (Xu & Deng, 1990). The five excavation sites are located along the main fault trace (Figure 3c). Trenches Tc01 to Tc04 cross the fault scarp where it is clearly visible, both in the field and in imagery. Tc02 is the same profile studied by Deng and Xu (1994), reexcavated in our study for direct comparison between their work and ours. Trench Tc05 is located at the foot of a triangular facet. Deposition in the five trench sites originates from several small catchments across the fault on the eastern hill slopes. Descriptions are given in section 4.2.

Clear evidence for earthquakes is provided in the trench by rupture scarps, scarp-derived colluvium, in-filled and open fissures, and offset sedimentary layers, in common with previous investigations of active fault zones (Liu-Zeng et al., 2007; McCalpin, 2009; Meghraoui et al., 2001; Ran et al., 2010; Sieh, 1978; Sieh et al., 1989; Sun et al., 2015). Upward terminations of faults are good indicators of surface faulting events. In this study, we find wedge-shaped deposits, interpreted as scarp-derived colluvium, to be particularly useful in identifying individual earthquakes.

3.3. AMS-14C Dating

In this paper, 31 samples for AMS-^{14}C dating from the five trenches (see section 4.2 for sample locations and descriptions and Table 2 for a summary of all results) have been collected and dated. Analyses were conducted at Beta Analytic Inc., USA, while detailed methods for sample preparation can be found at http://www.radiocarbon.com. Most of the result ages were calibrated using the INTCAL 04 database (Reimer et al., 2004). Calibrated radiocarbon ages are given in Table 2.

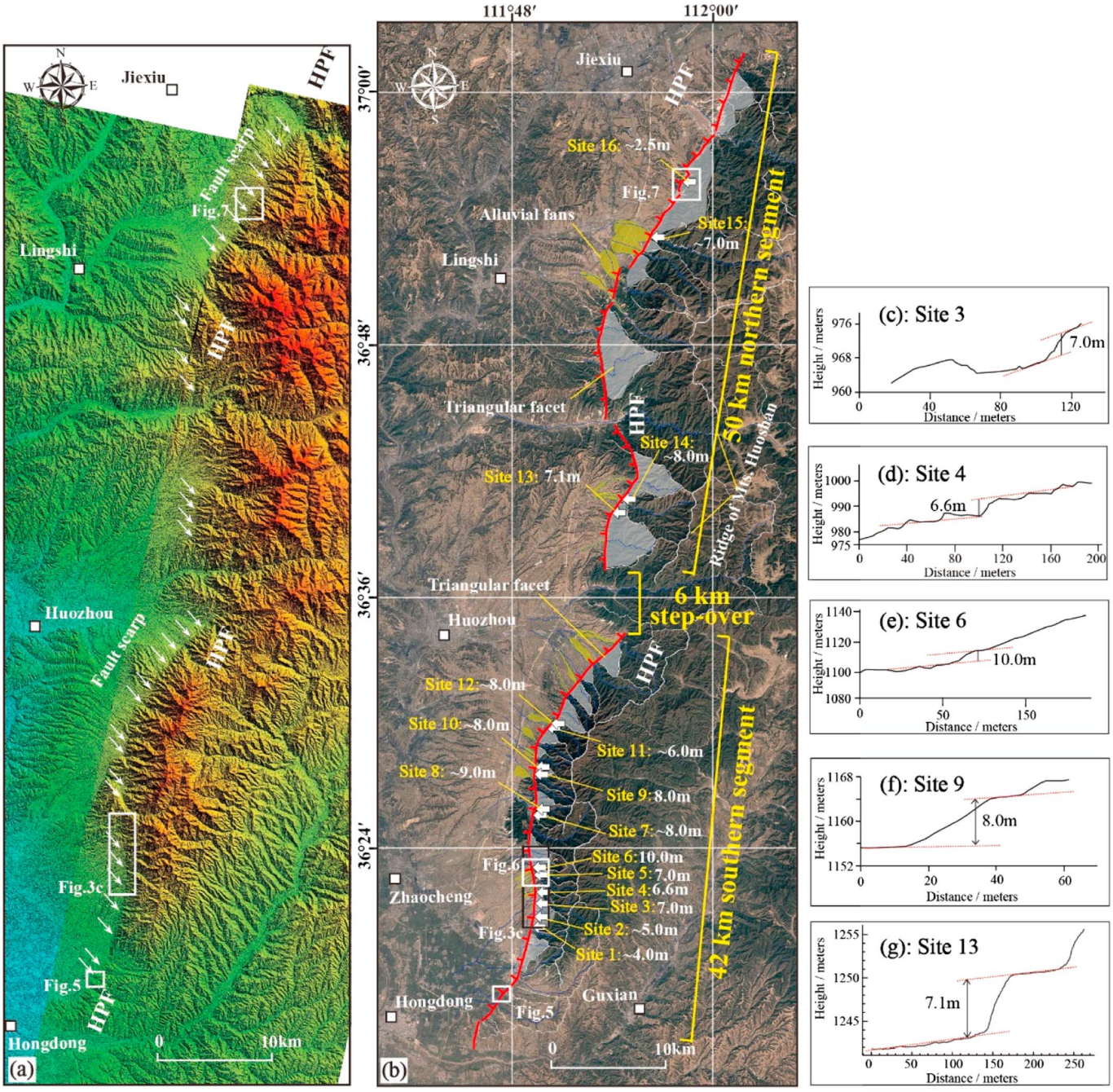

Figure 4. (a) High-resolution (3 m), digital elevation model of the Huoshan Piedmont Fault derived from IRS-P5 stereo imagery. (b) Google Earth imagery from June 2014 (source: http://earth.google.com) showing the distribution of the surface rupture related to CE 1303 Hongdong earthquake. The white arrows show the main measured vertical offset sites. The gray areas show main triangular facets; the yellow areas show the main alluvial fans. Note that the vertical offsets are cumulative displacements. (c–f) The measured vertical offset of the compound fault scarps.

4. Results

4.1. Geomorphology and Structure of the HPF

We mapped an end-to-end fault length of ~98 km, tracking the continuous expression of the most recent rupture event on the fault (Figure 4) toward the topographic limit of the scarp. The two ends of the fault were verified in the field. The northern end of the HPF is located south of the Taigu Fault (near 37.03°N, 112.03°E), while the height of the surface scarp related to the 1303 event decreases from ~2.5 m in Figure 7 to disappear

Table 2
Radiocarbon Ages and Calibrated Dates for the Samples From the Trenches Tc01 to Tc05

Sample	Lab no.	Radiocarbon age (year BP ± σ)	Calibrated years 2σ (CE or BCE)	Calibrated years 2σ (year BP)	Description	Unit sampled	Trench
n21	295,632	1,790 ± 40	140–380	1,810–1,570	Charcoal	U2a	Tc01
n31	295,633	4,030 ± 40	2,610–2,600 BCE	4,560–4,550	Charcoal	U6	
n37	295,635	1,080 ± 30	890–1,010	1,060–940	Charcoal	U2a	
n38	295,636	2,990 ± 40	1,360–1,350 BCE	3,310–3,300	Charcoal	U5	
n39	295,637	5,870 ± 50	4,840–4,610 BCE	6,790–6,560	Charcoal	U6	
n3291	296,968	26,380 ± 150			Organic sediment	U11b	
n3294	296,969	32,050 ± 230			Organic sediment	U11d	
n3295	296,970	4,150 ± 40	2,900–2,840 BCE	4,850–4,790	Organic sediment	U2b	
n3298	296,972	2,990 ± 30	1,400–1,260 BCE	3,350–3,210	Organic sediment	U3	
s1	295,638	50 ± 30	1,700–1,720	250–230	Charcoal	U1b	
s2	295,639	28,580 ± 150			Charcoal	U10	
xq3291	296,973	4,050 ± 40	2,850–2,810 BCE	4,800–4,760	Organic sediment	U11	Tc02
xq3292	297,730	4,590 ± 40	3,510–3420 BCE	5,460–5,380	Charcoal	U8	
xq3293	297,731	5,330 ± 40	4,320–4,290 BCE	6,270–6,240	Charcoal	U9	
xq3282	298,053	7,050 ± 50	6,060–5,890 BCE	8,010–7,840	Charcoal	U14	
xq3283	298,054		4,460–4,320 BCE	6,410–6,280	Charcoal	U4	
xq3284	298,055	6,350 ± 40	5,460–5,440 BCE	7,410–7,390	Charcoal	U13	
p1	295,641	38,280 ± 310			Charcoal	U28	T03
p4	295,642	41,680 ± 430			Charcoal	U17	
p7	295,643	570 ± 30	1,310–1,360	640–590	Charcoal	U5	
p8	295,644	340 ± 30	1,300–1,370	650–580	Charcoal	U2	
p10	295,645	840 ± 30	1,050–1,090	900–860	Charcoal	U6	
p14	295,646	10,240 ± 40	10,190–10,020 BCE	12,140–1,1970	Charcoal	U7	
p16	295,648	550 ± 40	1,310–1,360	640–590	Charcoal	U4	
p19	295,649	30 ± 30	1,640–1,670	310–280	Charcoal	U2	
p3291	297,737	41,270 ± 570			Organic sediment	U15	
p3293	297,738	6,180 ± 50	5,310–5,030 BCE	7,260–6,980	Organic sediment	U7	
sy4281	298,662	42,570 ± 570			Charcoal	U15	T04
sy42801	298,661	40,560 ± 480			Charcoal	U16	
syn3302	297,733	450 ± 30	1,440–1,500	510–440	Charcoal	U2	T05
syn3304	297,735	5,590 ± 40	4,490–4,340 BCE	6,440–6,290	Organic sediment	U7	

Note. All samples were prepared and analyzed by Beta Analytic Inc. (Miami, Florida, USA). All of the raw radiocarbon ages are calibrated by INTCAL 04 database (Reimer et al., 2004), with 2 standard deviation uncertainty and a confidence level of 95%. Radiocarbon ages expressed as BP relative to 1950 years. All details of sample analyses are available in the supporting information.

at the northern end of Mount Huoshan (Figure S5). The southern end of the fault is located east of Hongdong (near 36.24°N, 111.75°E) (Figures 2 and 4); the height of fault scarp is 2.0 m in Figure 5, but disappears within the basin to the south (Figure S2), where sand liquefaction structures are present (Meng et al., 1985; Xu & Deng, 1990). The 98 km estimate is the likely maximum, given the lack of further topographic traces. The real length may be smaller, given that we did not observe definite 1,303 ruptures within 15 and 5 km of the northern and southern topographic limits of the scarp.

At 104 individual localities, we observed the main fault plane; overall strike is N0°E–N30°E, dipping at 55°85° (Figure 2d). Among the localities, there are 10 sites with 20 groups of exposures of fault striations. Striations pitch in a range of −60°–108° (Figure 3b), and so record dip-slip faulting, with a minor oblique-slip subset.

We identified one step over (relay) zone about 6 km east of Huozhou (Figure 4). This step over marks the transition between two main segments of the HPF, the northern and southern segments, respectively. Along this step over, we found faults along the boundary between alluvial fans and piedmont loess hills, but not obvious fault scarps related to recent activity. The step over is exploited by one of the main rivers to cross the Huoshan (Figure 3a), also suggesting that it has a long-term importance and is not simply a break in the rupture trace of the Hongdong event.

The southern segment of the HPF is ~42 km long (see Figures 3 and 4a for location). A series of fault scarps lie adjacent to the mountain front. There are a series of triangular facets and alluvial fans distributed along the

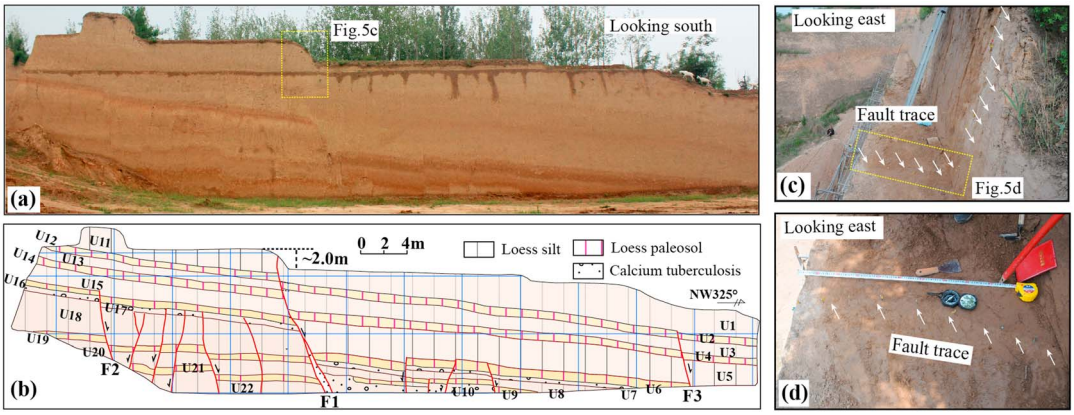

Figure 5. (a) Photograph showing a 40-m long section through the main fault (36.27°N, 111.78°E). Note that the location of the main fault trace is consistent with the fault scarp. (b) Sketch of the same view as in Figure 5a showing the principal units and their relationship with faulting. F1 cuts every unit in the profile, and its breakpoint extends to the surface, while the secondary faults only cut the lower units of the section. (c and d) Photographs showing the fault trace near the upper part of the section.

fault segment. South of Guangshengsi, several outcrops of fault planes, modified fault scarps, and sand liquefaction sites lie along the main fault trace. Figure 5 shows a locality (at 36.28°N, 111.78°E), where the main fault extends to the surface with a scarp ~2 m high south of Guangshengsi. Figure 6 shows part of the southern fault segment where a linear compound scarp of ~10 m height is visible, located at the edge of an alluvial fan (see section 4.2.3). The scarp cuts the terrace of the river crossing it (Figure 6d). Figures 6c and 6d show that the fault plane cuts a late Pleistocene unit and extends to the surface. Along the southern segment of HPF, we found 12 sites with fault scarps, located at the edge of corresponding alluvial fans; the height of the cumulative scarps ranges from 4.0 to 10.0 m (Figure 4b), while the single-event scarp is ~2.0 m (Figure 5b). Within the southern segment, we found dozens of fault plane exposures located close to each trench profile, and also along the banks of rivers that cross the fault.

The northern segment of HPF is ~50 km in length (Figures 3a and 4b). We measured the scarp at 4 sites, with heights of 2.5–8.0 m. These are cumulative scarps, with the exception of the 2.5 m scarp, which relates to a single event. We also found four sites with fault striations; the pitch ranges from −71° to 108°, meaning mainly dip-slip motion (Figure 3b). Figure 7 shows part of the northern segment (at 36.92°N, 111.97°E) (Figure 3a). A fresh fault scarp was seen in the field and can be followed across loess hills located at the foot of the triangular facet (Figure 7c). The fault plane extends to the surface.

As well as the main northern and southern segments of the HPF, which are picked out by the two rupture segments of the Hongdong event, there are four en echelon, left-stepping segments (Xu et al., 1993) (Figure 3a). Segment junctions are located at 36.85°N, 111.91°E; 36.74°N, 111.92°E; 36.64°N, 111.89°E; and 36.46°N, 111.82°E. In each case breaching of the step over has occurred by propagation of the rear fault, leaving segment ends that did not rupture in the CE 1303 event (compare Figures 3a and 4b).

4.2. Paleoseismology Study

Results are reported from the trench sites from south to north.

4.2.1. Trenches Tc01 and Tc02: Observations

The site of Tc01 and Tc02 is located along the southern segment of the HPF, 17.6 km northeast of Hongdong (Figure 3c). There are well-developed landforms indicative of normal faulting on the fault, such as a linear fault scarp with vertical height of ~7 m, and many fault surfaces exposed in the adjacent river valleys. Deposits at this site are mainly loess and weathered colluvium, which was transported from nearby hillslopes. Trench Tc01 (36.36°N, 111.81°E) is located near the middle of the fault scarp, with no nearby channels. Trench Tc02 (36.36°N, 111.81°E) is 5 m north of Tc01 and is a reexcavation of an earlier trench dug by Deng and Xu (1994).

Trench Tc01 is ~20-m long, 1.5-m wide, and on average ~4-m deep. Tc02 is ~7-m long, 2-m wide, and 3-m deep. Both trenches provided exposure sediments as old as the late Pleistocene (see dating descriptions).

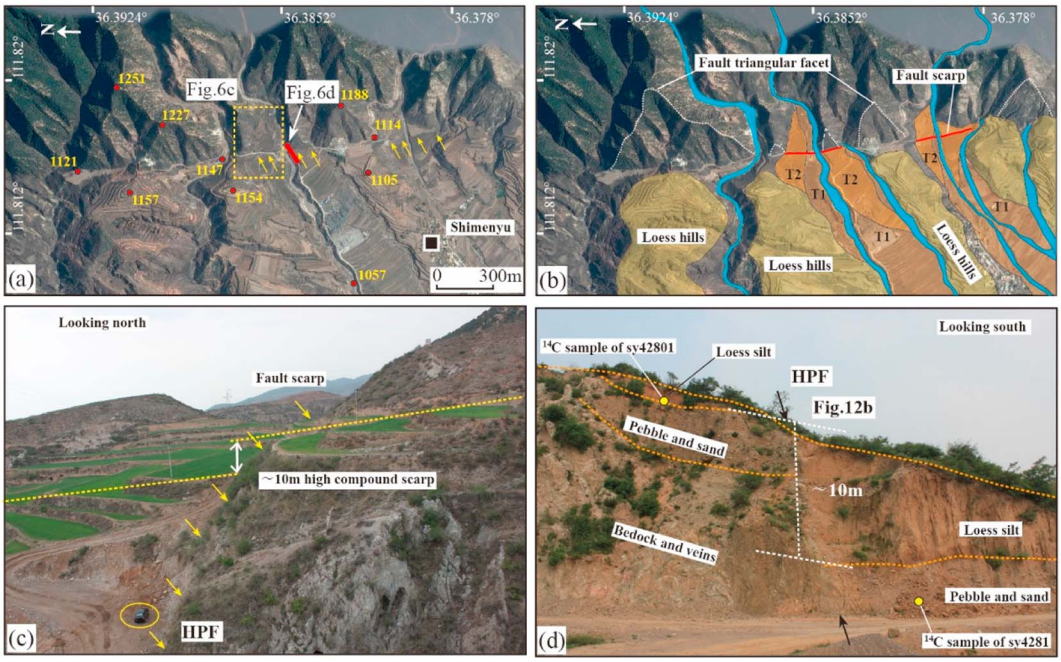

Figure 6. (a) Google Earth imagery from October 2016 (source: http://earth.google.com) of several rivers crossing the Huoshan Piedmont Fault near Shimenyu village. Fault scarp marked by yellow arrows. (b) Annotated geomorphologic map of the same site, showing different generations of alluvial fan surfaces and loess hills. Scarps are marked by a thin red line and triangular facets by a white dotted line. (c) Field photograph showing the fault scarp located at the apex of an alluvial fan. Vertical displacement is ~10 m. Note the sport utility vehicle car in the yellow ellipse for scale. (d) Photograph showing the fault profile, which has dislocated the second youngest terrace (T2) by ~10 m.

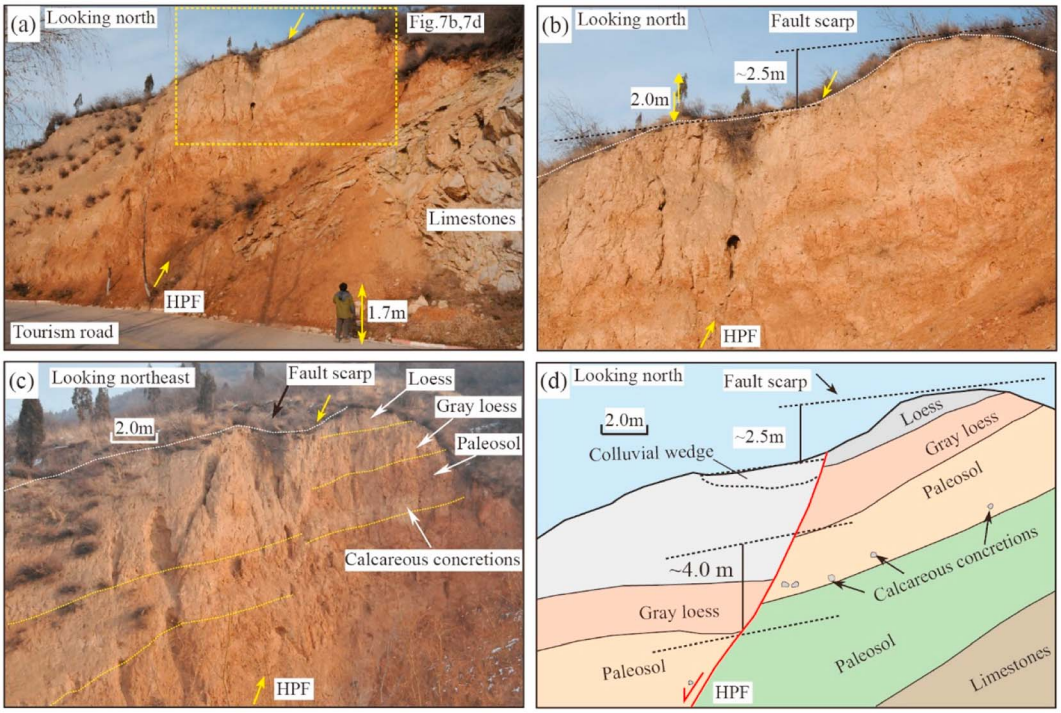

Figure 7. (a) Field photograph (36.92°N, 111.97°E) showing a cross section through the main HPF. The fault trace is marked by yellow arrows. The fault reaches the surface, offsetting the loess layers. (b and c) Field photographs to show the relationship between the fault scarp and fault plane. (d) Sketch of the same view as in Figure 7c indicating the principal units exposed in this section. Note the dislocated grey loess layer with ~4 m displacement, and vertical scarp with height ~2.5 m.

Each trench wall was cleaned, gridded into 1 m × 1 m squares, observed, and photographed. Detailed mapping of trench exposures was performed on printouts of photographs of the grid cells (Figures 8 and 9).

Figures 8c and 8e show an overview of the stratigraphy exposed on the north profile and south profile of trench Tc01, respectively. The strata of both walls are similar and hence are correlated to each other (Figures 9a and 9b). Neither profile exposes bedrock. The unconsolidated sediments consist of loess, poorly sorted gravel, clay, and paleosol. Based on the similarity and contrast of texture, color, and facies, the stratigraphy of trench Tc01 is divided into 11 units, numbered in ascending order U11–U4, and U1, while U3 and U2 are identified as colluvial wedges.

Four main faults are identified and named F1 to F4 (Figures 8d and 8f). F1 dips northwest and forms the main tectonic contact between the hanging wall, with mainly Holocene sediments, and the footwall, with mainly late Pleistocene sediments. F2 is similar to F1 in geometry, dipping steeply northwest, but only appears in Pleistocene sediments. F3 and F4 are located west of F1, and dip southeast, opposite to F1. The main fault F1 dips at 77°. The nearby topographic scarp is 7.0-m high, interpreted as the direct result of seismic slip during Holocene earthquakes. These values give a slip of 7.2-m along the scarp face, assuming pure dip-slip motion.

The 11 sedimentary units are in two categories, those which are wedge-shaped in cross section (U9, U3, and U2), and those which are more stratified and laterally extensive (all other units). U10 and U11 are cut by F1 and F2 and do not appear west of these faults; their eastern limits are uncertain. Both units show clear sedimentary stratification. U9 contains mixed gravel and sand and is distinctly wedge-shaped along the trench profiles; it covers fault F2. U7 is exposed from west of F1 across the rest of the trench and consists of fine yellow silt (loess) deposits. U6 and U5 are of similar extent along the trench walls as U7, but successively coarser (Figures 8d and 8f). U4 is thin gravel, conformable above U5. U3 is a 3-m thick, wedge-shaped unit, found adjacent to F1, which contains organic material, gravel, and a massive paleosol. U2 is also a wedge-shaped unit, with variable sediments, bounded like U3 by fault F1 (Figure 8a). U1 drapes across fault F1 and is the surficial soil and gravel.

Three samples, n3291, n3294, and s2, were collected from U10 and U11 in trench Tc01 and yielded late Pleistocene ages of 28,580 ± 150 year BP (U10), and 26,380 ± 150 year BP to 32,050 ± 230 year BP (U11). Samples from U1 to U7 yielded ages younger than 6,790 year BP. Sample n3295 from U2 has an age considerably older than the ages from the rest of U2 (sample n37: 1,060–940 year BP and sample n21: 1,810–1,570 year BP) and is probably detritus reworked from older deposits (Figure 9). We exclude this sample from further discussion. For the same reason, samples n3298 from U3 and n37 from U2 may also be reworked from older deposits, but the sample ages can be used to constrain earthquake events, which cannot be older than these ages, see below.

Figure 10a shows an overview of the stratigraphy of trench Tc02. Strata consist of poorly sorted mixtures of gravel and sand, which are different from adjacent trench Tc01. The stratigraphy can be divided into 18 roughly tabular units (U18–U5, and U1 in ascending order) (Figure 10b), while U4–U2 are identified as colluvial wedges.

In trench Tc02, three faults are identified, named F1 to F3 from east to west (Figure 10b). F1 is similar to F2 in geometry; both faults dip steeply west. F3 dips east in its upper part, but changes orientation at the base of U4 to dip west, and runs parallel to F2 to the bottom of the trench. F2 is the most prominent fault in Tc02.

Six samples yielded ages younger than 8,010 year BP (Figure 10b). Samples xq3282, xq3284, and xq3291 are from U14, U13, and U11, respectively, in the footwall of F1 and F2, while samples xq3293 and xq3292 are from U9 and U8, respectively, in the hangingwall of F1 and F2. Sample xq3283 is from U4.

4.2.2. Trench Tc03: Observations

Trench Tc03 (Xingwangyu, 36.36°N, 111.81°E) is located on an alluvial fan, <400 m north of Tc01 and Tc02 and 18 km northeast of Hongdong (Figure 3c). Near the trench, there is a well-developed fault scarp crosscutting the fan with height 6.6 m (Figure 11a). This is interpreted to be a cumulative scarp, recording slip from more than one earthquake, partly by comparison with the 7 m scarp at Tc01. Tc03 was excavated from a natural channel wall (Figure 11b).

Trench Tc03 has an average height of ~12 m and is ~40-m long. The trench profile was processed in the same way as described for Tc01 and Tc02, but gridded into 2 m × 2 m^2. Figure 11c shows the exposed stratigraphy.

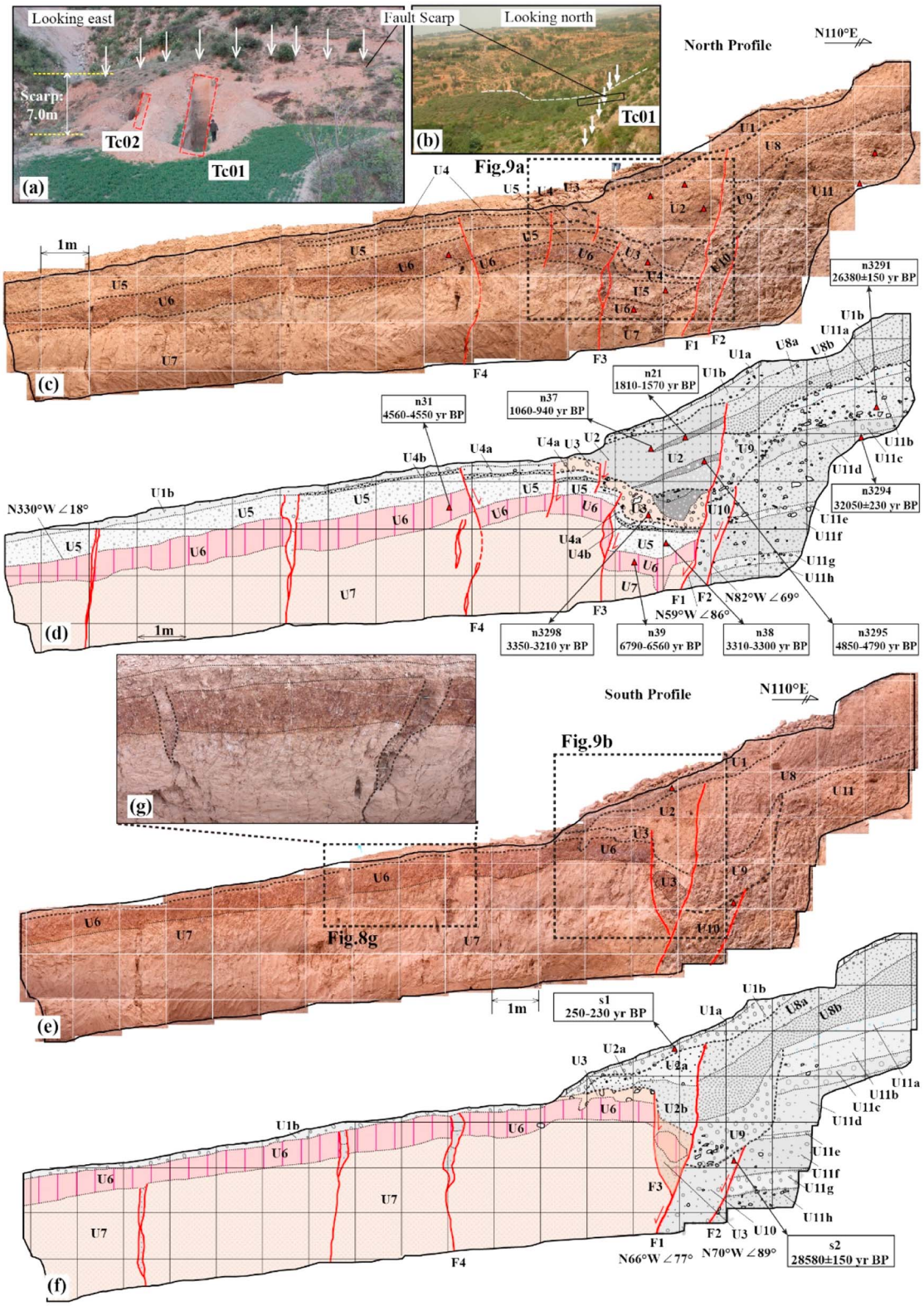

Figure 8. (a and b) Field photographs showing details of trenches Tc01 andTc02, including the adjacent ~7-m fault scarp; the white arrows show the top of the scarp. (c) Photographic mosaic and the (d) interpreted map of the North profile of Tc01. (e) Photographic mosaic and the (f) interpreted map of the South profile of Tc01 (mirrored), and (g) the photograph shows details of south profile. "U" denotes stratigraphic unit, and the black dashed lines show the stratigraphic contacts. The red lines indicate fault planes. The small red triangles show the locations of radiocarbon samples, labeled with sample numbers and their corresponding corrected radiocarbon ages (2σ) (Table 2).

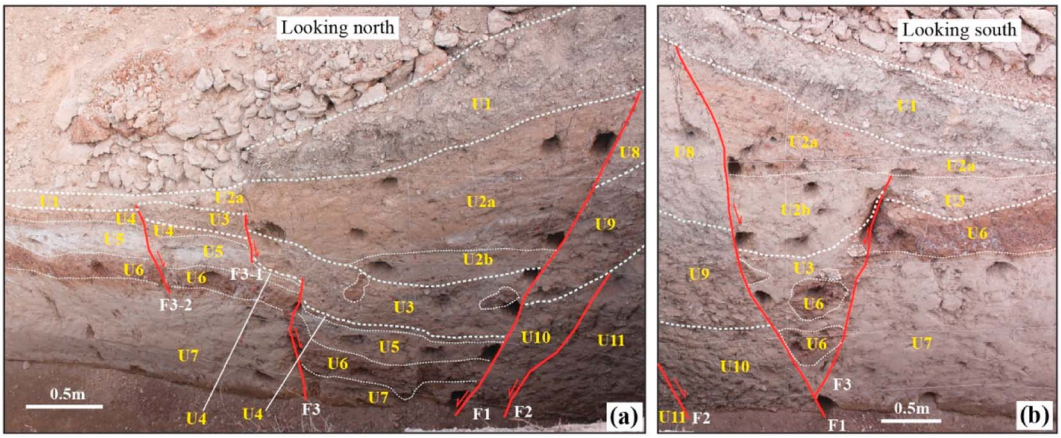

Figure 9. Close-up photographs showing the details of the (a) north profile and (b) south profile of the Trench Tc01 exposures; see location in Figures 8c and 8e, respectively.

The sediments consist mostly of gravel and sand transported from the adjacent catchment in Mount Huoshan, with loess and a paleosol at the top of the profile. The stratigraphy is divided into 28 units, which are numbered in an ascending order from the top to the bottom (Figures 11c and 11d). Figure 11 shows units U28–U19 in the footwall and U9 to U1 in the immediate hangingwall of F1 and F6, with U18 and U10 west of F6. A single wedge-shaped unit, U5, occurs between F1 and F2.

Nine faults are identified: F1 to F9 from east to west (Figure 11c). There are two small grabens associated with F1 and F3, F8 and F9, respectively. The upper fault tips of F5 to F9 are buried by U6. F1 cuts U28 to U22 and is the main fault in the profile. F2 cuts U8, U7, and U6 and terminates at the base of U5 and U4. F3 cuts U7 and U6 but is covered by U3.

Numerous charcoal and other organic sediments were found in Tc03. Ten samples were dated. Samples p1 collected from U28, p4 collected from U17, and p3291 collected from U15 yielded late Pleistocene ages. Samples collected from U4 to U2 yielded ages younger than 640 year BP. Sample p10 collected from U6 yielded an age 900–860 year BP, that is, older than the CE 1303 earthquake. Sample p7 collected from U5 yielded an age close to CE 1303, at 640–590 year BP (noting that BP is taken as CE 1950).

4.2.3. Trench Tc04: Observations

Trench Tc04 (36.38°N, 111.81°E) is located at the edge of an alluvial fan near Shimenyu, 2.1 km north of Tc03 (Figure 3c), 19.3 km northeast of Hongdong. Near site Tc04, a fault scarp cuts fan sediments with vertical offset of ~10 m. The fault scarp and triangular facets (Figure 6d) indicate the fault trace clearly. The trench profile is cleaned from a natural channel (Figure 12a).

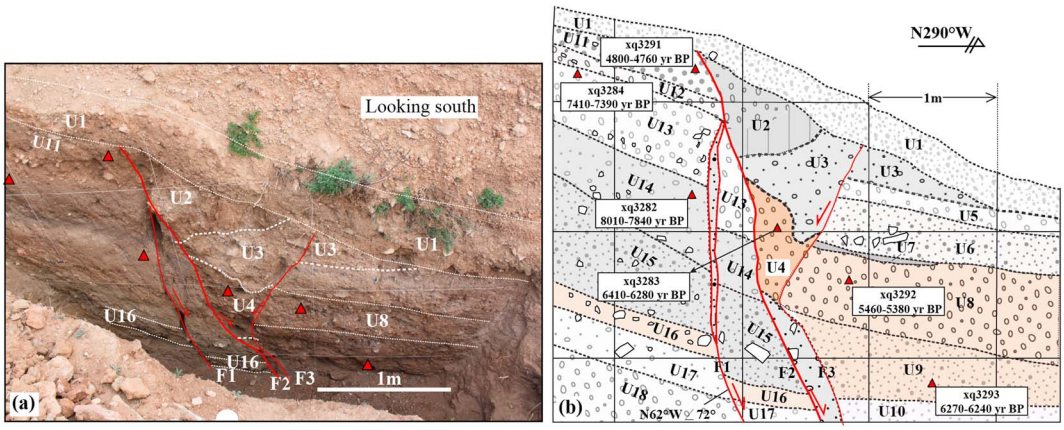

Figure 10. (a) Photograph and the (b) interpreted map of the profile of Tc02, depicting the stratigraphy and faults. Sample numbers and their corresponding corrected radiocarbon ages (2σ) are labeled (Table 2).

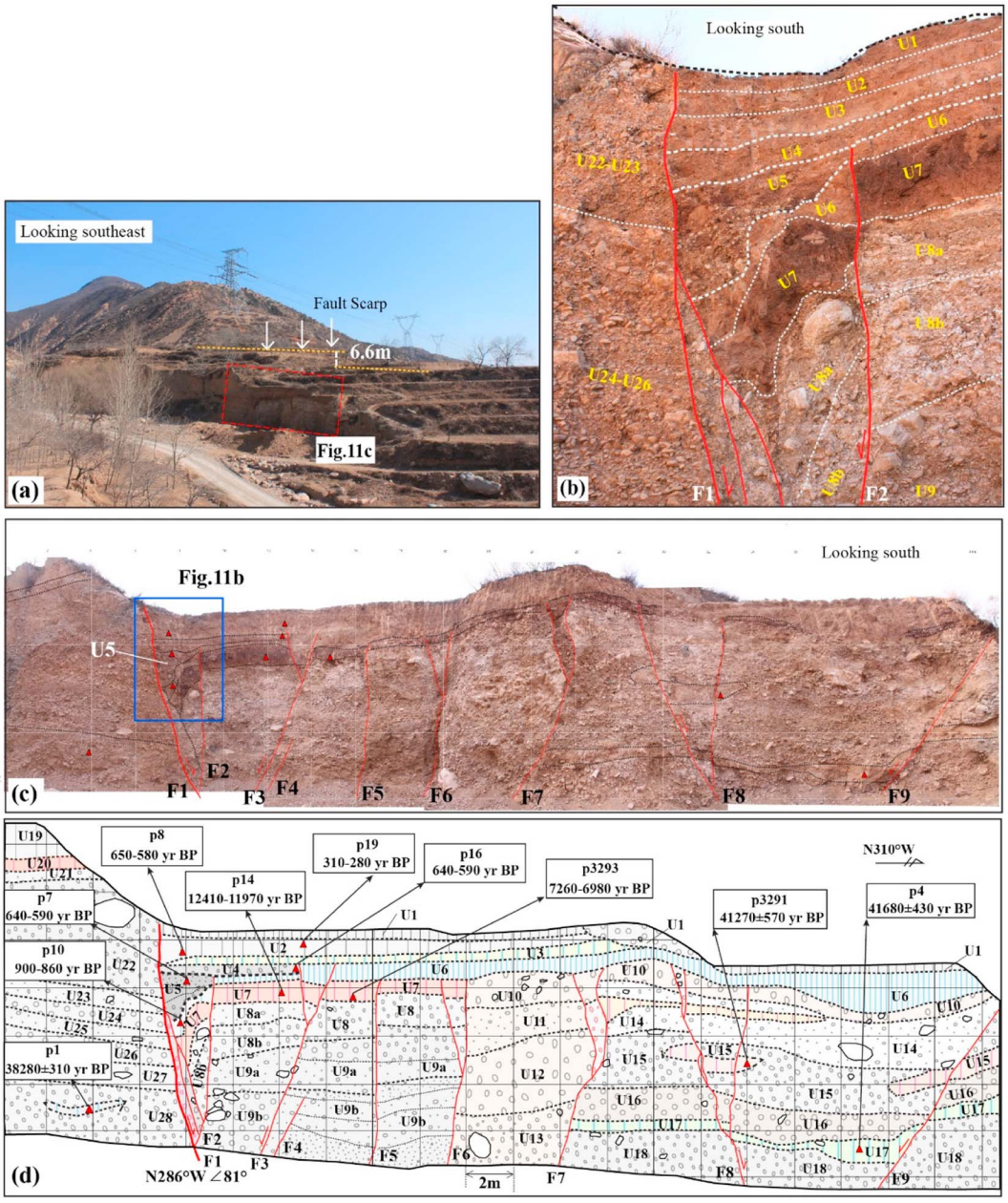

Figure 11. (a) Photograph showing the trench Tc03 site location. (b) Enlarged photograph shows F1 and F2 dislocating units U6 to U8, and forming the wedge-shaped unit of U5. (c) Photographic mosaic and the (d) interpreted map of the profile of Tc03, depicting the stratigraphy and faults. Sample numbers and their corresponding corrected radiocarbon ages (2σ) are labeled (Table 2).

The trench is ~50-m long and has a maximum depth of ~20 m. The trench profile was processed in the same way as described for Tc03, focusing on the main fault area. Figure 12b shows an overview of the exposed stratigraphy; Figure 12c shows the detail at the top of the trench. The bedrock (U18 and U19) in the footwall consists of Archean gneiss and dikes, both strongly sheared and fractured. The unconsolidated sediments overlying the bedrock are composed mainly of unsorted mixtures of pebbles and sand with muddy cement, also loess and paleosol. The stratigraphy is divided into 19 units, U19–U1, which are stratified and vary in their grain size and color, and a single wedge-shaped U2, at the top of the trench adjacent to F1 (Figure 12c).

In Tc04, one fault is present from the top to the bottom of the trench, named F1 (Figure 12b). Two other adjacent faults are present at the top of the profile, named F2 and F3 (Figure 12d).

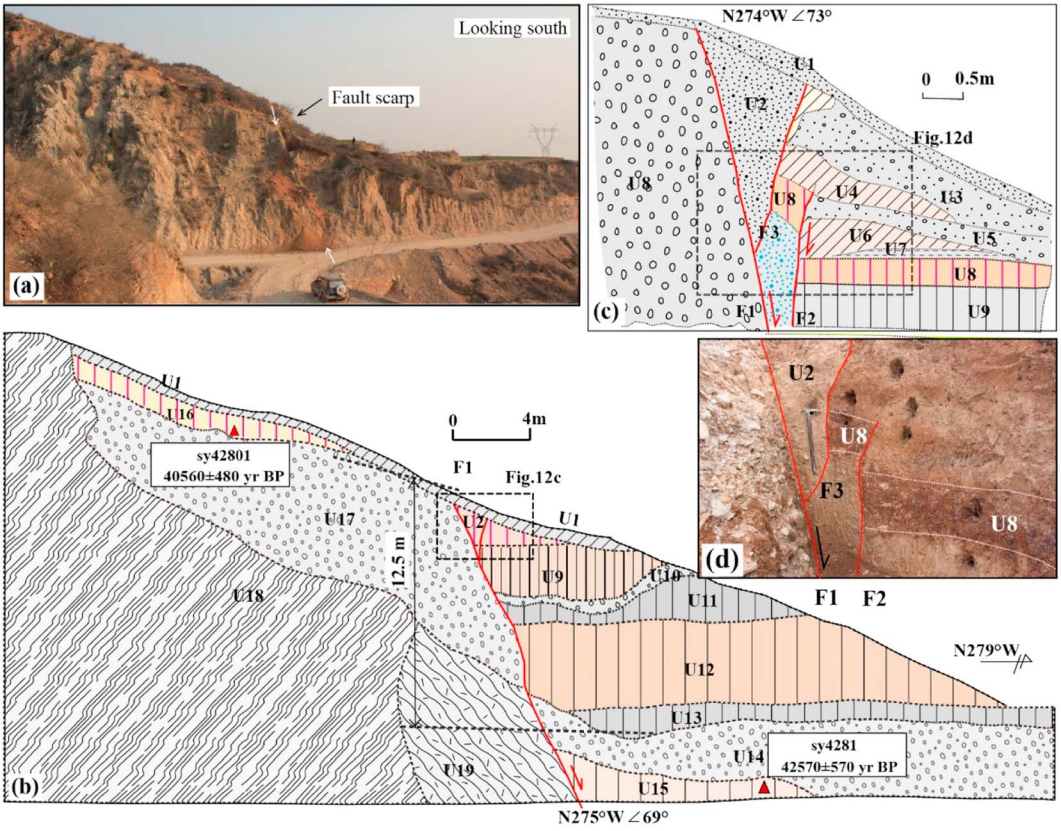

Figure 12. (a) Photograph showing the Tc04 site (see Figure 6d for another photograph of this site). (b) The interpreted section. Sample numbers and their corresponding corrected radiocarbon ages (2σ) are labeled (Table 2). (c and d) Close-up photograph and interpretation showing the fault at the top of the profile; note that F1 reaches near the surface and wedge-shaped unit U2 is only covered by U1, probably showing the CE 1303 event.

Two samples were collected from the trench Tc04; radiocarbon dates are summarized in Table 2. Sample sy4281 from U15 and sy42801 from U16 yielded ages similar to U15 and U17 in Tc03.

4.2.4. Trench Tc05: Observations

The north Shimenyu site Tc05 (36.39°N, 111.81°E) is also located at the central section of the southern segment of the HPF, 3 km north of Tc01, 20.0 km northeast of Hongdong. Around the site, there are well-developed landforms indicative of normal faulting on the fault, such as fault scarps and triangular facets (Figure 3c). The trench is cleaned from a quarry profile (Figure 13a). Tc05 is ~15-m long and ~7-m deep; it provided exposure of both Quaternary sediments and bedrock. The trench wall was prepared and analyzed in the same way as Tc01 and Tc02.

Figure 13d shows an overview of the stratigraphy exposed in the profile. Weathered Archean gneiss (U9) is exposed at the eastern end. Unconsolidated sediments overlying the bedrock consist mostly of poorly sorted mixtures of gravel, sand, loess, and paleosol. U2 has a distinct wedge-shaped profile in cross section and consists of a mixture of clay and gravel. The other Quaternary units are more stratified and consist of variable amounts of gravel, sand, silt, clay, and remnants of paleosol. There is a veneer of green-colored fault gouge distributed over the fault plane.

Six faults are identified and named F1 to F6 (Figure 13d). There are several small-sized grabens in the profile. Unit U2 is associated with both F1 and F2, forming a V-shaped collapse wedge, which contains a mixture of unsorted gravel, sand, and paleosol, Another small graben is associated with both F3 and F4, which is filled with U3. F3 and F6 cut U6 and U7, forming a graben that filled with U5 and U4.

Two samples were collected and analyzed from trench Tc05. Sample syn3304, collected from U7, yielded an age of 6,440–6,290 year BP, consistent with the paleosol units U7 in Tc03 and U6 in Tc01. Sample syn3302, collected from U2, yielded an age younger than the CE 1303 Hongdong earthquake (510–440 year BP).

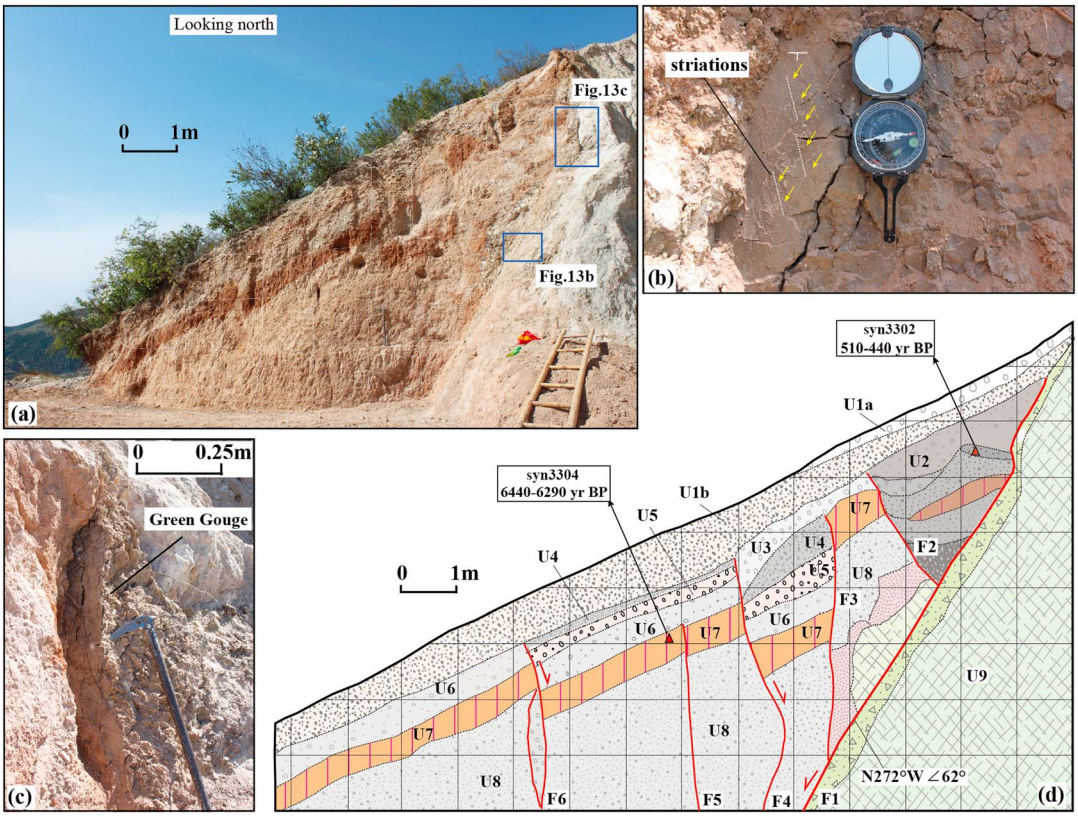

Figure 13. (a) Photograph showing Trench Tc05. (b) Photograph showing striations along the fault plane; the pencil is aligned parallel to the striations. (c) Photograph showing green fault gouge along the fault plane; (d) the interpreted section. Sample numbers and their corresponding corrected radiocarbon ages (2σ) are labeled (Table 2).

4.2.5. Trenches Tc01 and Tc02: Interpretation

Three earthquake events are identified in the exposures of both walls of Tc01. The youngest event occurred before the deposition of U2 and after that of U3, using the wedge-geometry of U2 to interpret this deposit as a colluvial wedge, that infilled a scarp produced by a rupture along F1.

We use our AMS-^{14}C ages to provide absolute age constraints on the earthquakes identified in this study. It is clear where strata predate or postdate the colluvial wedges, which are interpreted to form as a result of each event. Organic material may be reworked in any unit, leading to ages that are spuriously old. The colluvial wedges themselves are assumed to begin to accumulate immediately after the rupture but are not instantaneous. Ages of samples from the wedges may therefore predate the causative earthquake, or postdate it, but only by the time it took to accumulate the wedge itself. As we bracket earthquake ages in this and following sections, we note whether the age constraints are from prewedge strata, the wedge itself, or strata that overlie the wedge. Ideally, dates would be available from three horizons: above, below, and within the wedge itself; this is not always the case. We give emphasis to ages from the wedges themselves, given that these formed as a direct consequence of major earthquakes, whereas prewedge and postwedge strata provide maximum and minimum constraints.

Using the approach outlined above, the age of the youngest event in Tc01 and Tc02 is constrained to be between 1,060 and 230 year BP, which is the interval between the youngest ages from samples in U2 (the colluvial wedge) and U1 (the overlying surficial deposits).

The second-youngest event occurred after the deposition of U6–U4 and before U3, interpreting U3 as a colluvial wedge produced by the rupture. The age of the second event is ~3,310–3,210 year BP, using the ~3,350–3,210 year BP age of the wedge and the 3,310–3,300 year BP age of underlying unit U5. The third (oldest) event occurred before U9 and after U10, again using the wedge-shaped geometry of U9 as a key marker, and interpreting this unit as the oldest colluvial wedge preserved at this trench. The age of this

event is not well-constrained because of a lack of samples. Given that U11 predates the event, we infer a late Pleistocene earthquake younger than the age of sample n3291 from U11b: 26,380 ± 150 year BP.

We also identify three paleoseismic events inTc02 based on the wedge-shaped sediment packages U2–U4, each of which is interpreted as a colluvial wedge corresponding to an individual earthquake. The timing of the three events recorded in Tc02 is partially constrained by the trench samples, but inference from Tc01 is also needed. The age of the youngest event in Tc02 occurred before the deposition of U2 and after that of U3. No samples were dated from Tc02 to constrain the date of U2 directly; we use the result from Tc01 of 1,060–230 year BP, assuming that the youngest wedge-shaped packages in Tc01 and Tc02 are directly equivalent.

The age of the second event in Tc02 occurred before the deposition of U3 and after that of U4, U11, and U12. The only direct constraint from Tc02 is that this event is younger than the age of sample xq3291 from U11, that is, <4,800 year BP. The age of the third event in Tc02 occurred before the deposition of U4, and after deposition of U8, U9, and U13; thus, it was younger than the 5,460–5,380 year BP age of sample xq3292.

4.2.6. Trench Tc03: Interpretation

There is one clear earthquake recorded in Tc03, on fault F1 (Figure 11d). The timing of this event is bracketed by dates on units U6 (preevent) of 900–860 year BP and U5 (colluvial wedge) of 640–590 year BP. U1–U4 seals other faults (F4–F9), which offset strata in the hangingwall of F1, but the age control on the faulting is not precise. Faults F2–F6 cut U7, for which sample p3293 yielded an age of 7,260–6,980 year BP. Therefore, we conclude that one or more events affected the sediments in Tc03 in the time interval 7,260–900 year BP.

4.2.7. Trench Tc04: Interpretation

Only one event is identified in this trench, interpreted to have formed by slip on fault F1 before deposition of the wedge-shaped unit U2. There are no direct age constraints, because the only two samples dated from this trench yielded late Pleistocene ages of ~40–42 kyr BP, and come from strata well below U2 (Figure 12b). The U14 and U17 are the same unit for both are composed of the same lithology of mixed and unconsolidated sand and gravel; we measured the 12.5 m offset based on the top surface of both U14 and U17, and the U17 sits on top of bedrock in the footwall of the HPF, consistent with normal faulting during the late Pleistocene and Holocene; U14 is in the hangingwall and was deposited over Pleistocene sediments (U15). The sample ages constrain the approximate age of U14 and U17, which is offset vertically ~12.5 m by F1. The implication is that F1 has a low late Quaternary slip rate, of <1 mm/year.

4.2.8. Trench Tc05: Interpretation

Three earthquakes are interpreted from the record of this site (Figure 13). Wedge-shaped unit U2 records the youngest and best-constrained event, along fault F1. Sample syn3302 from U2 is dated at 510–440 BP, suggesting an event comparable to this age range. Two other older events are recorded by wedges U3, and U5, respectively, but they are undated, except for the constraint that they both postdate offset unit U7 (6,440–6,290 year BP).

5. Discussion

5.1. Earthquake Correlation and Recurrence Interval

Four earthquake events found in the five trenches across the southern segment of the HPF can be summarized as follows (Table 3). One event is clear in all five trenches, based on colluvial wedges preserved adjacent to the main fault in each trench, near the surface. We refer to this earthquake as Event E1.The age is constrained within the range CE 990–1,360 (1060–590 year BP), based on AMS-^{14}C ages of material within and bracketing the wedge-shaped packages in Tc01, Tc03, and Tc05. This event clearly corresponds to the CE 1303 Hongdong earthquake. No other unique events can be distinguished in Tc03 and Tc04. Two older events are recognizable in each of trenches Tc01, Tc02, and Tc05.

Event E2 is identified in trenches Tc01, Tc02, and Tc05, assuming that the second wedge-shaped package of sediment in each trench represents the scarp fill of the same earthquake. The age of this event is only well constrained by AMS-^{14}C ages from Tc01. Preevent sediment (U5) and the wedge-shaped unit U3 bracket the event to 1,360–1,260 Before Common Era (3,310–3,210 year BP).

An event happened after the deposition of reddened (paleosol?) units U8–U9 in trench Tc02, which are dated at 6,270–5,380 year BP (5,460–5,380 year BP for the youngest sample). In Tc05, there is an event postdating a

Table 3
Summary Radiocarbon Age Estimates for Major Earthquakes E1–E4 on the HPF, by Trenches Tc01–Tc05

	E1 (CE 1303)	E2	E3	E4
Tc01	1060–230	3,310–3,210	Not recorded	<26,380
Tc02	Present, but age not constrained	<4,760	<5,460–5,380	Not recorded
Tc03	640–590	?	<6,980?	?
Tc04	Present, but age not constrained	?	?	?
Tc05	510–440	?	<6,290?	Not recorded
Preferred age range	1060–590	~3,310–3,210	<5,460–5,380	<26,380

Note. Ages in years BP.

paleosol (U7) dated at 6,440–6,290 year BP. We suggest that these trenches record the same earthquake, E3, possibly displacing an equivalent mid-Holocene paleosol horizon. E3 therefore has an age of <5,460–5,380 year BP.

Another event E4 is recorded only in Trench Tc01. It postdates horizon U11a, dated at 26,380 ± 150 year BP, and predates a mid-Holocene paleosol dated at 6,790–6,560 year BP (U6; sample n39). For this reason we argue that it is a different event to E3, but the age is not well constrained.

Overall, there is a record of three strong earthquakes along the southern segment of the HPF since the mid-Holocene. The interval between each event is roughly 2,000–3,000 years.

The sequential deformation and deposition of stratigraphy before, during, and after events E1 and E2 in Tc01 are shown in schematic form in Figure 14. Figure 15 shows the equivalent diagram for the sequence E3–E1 for Tc05. In each case, a sequential restoration can be performed on the present trench structure, leading back to the preearthquake stratigraphy. The ability to restore the sections in this way gives confidence in the interpretation of the stratigraphy and shows that a dip-slip motion on the fault is consistent with the present structure.

5.2. Characterizing the CE 1303 Earthquake

5.2.1. Identification of the Causative Fault

In section 4.2, we showed that the most recent earthquake in trenches Tc01, Tc03, and Tc05 can be constrained to 1,060–590 year BP by AMS-^{14}C dating. In section 4.1, we described recent scarps along the foothills of Mount Huoshan. Based on these observations, we conclude that the HPF ruptured during the CE 1303 Hongdong earthquake, as previously suggested by other studies (Deng & Xu, 1994; Jiang et al., 2004; Meng et al., 1985; Xie et al., 2004; Xu & Deng, 1990).

Our study reveals a rupture ~98-km long. Our study does not by itself show that the HPF was the only fault to have ruptured during the CE 1303 event, which has a major bearing on the magnitude of the earthquake. The Taigu Fault on the east side of the Taiyuan Basin (Figure 2a) is also an active fault. On the basis of gullies interpreted to be offset in a right-lateral sense along the Taigu Fault, some authors have attributed the CE 1303 event to the combined the HPF and Taigu Fault, with a surface rupture zone estimated at 160 km in length (Jiang et al., 2004; Xie et al., 2004).

However, paleoseismicity studies of the Taigu Fault do not indicate it slipped during the CE 1303 event. Trenching work by Xie et al. (2004) showed the latest faulting event at similar times to ^{14}C ages of 3,350 ± 150 and 4,450 ± 170 year BP. There is no evidence to support activity related to the CE 1303 event. Jing et al. (2016) found the latest paleoseismic event to be at ~8 ka using the Optically Stimulated Luminescence (OSL) dating ages, that is, in the early Holocene (see the supporting information). In addition, recent fault mapping work by Xu, Shen, et al. (2011) suggested that the latest event on the Luoyunshan Fault, to the south of the HPF, was at 7.52 ± 0.1 ka BP, that is, in the early Holocene.

The isoseismals of the CE 1303 event are elongate parallel to the HPF (Figure 2), with a distribution that does not implicate rupturing of the Taigu Fault and/or the Luoyunshan Fault. The combined dating evidence from the Taigu and Luoyunshan faults complements our results and the isoseismal evidence and suggests that the HPF was the only fault to rupture in the CE 1303 Hongdong earthquake.

Slip sense during the CE 1303 event and over longer time periods has been debated, with both normal dip-slip (State Seismological Bureau (SSB), 1988; Xu et al., 2013; Xu, 2013) and dextral strike-slip (Hu et al.,

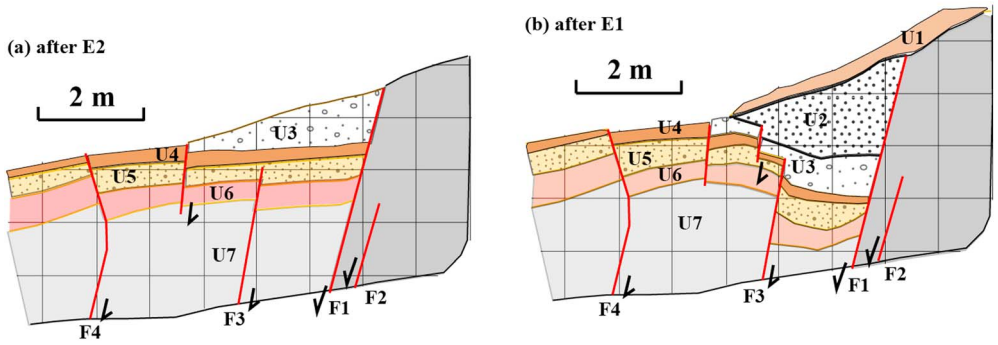

Figure 14. Schematic diagram of paleoearthquake sequence derived from the north profile of Trench Tc01. (a) After event E2, the colluvial wedge of U3 formed, and U5 and U6 were tilted by faulting. (b) After Event E1, the colluvial wedge of U2 formed, U3 was faulted by F1 and F3.

2010; Jiang et al., 2004; Xu & Deng, 1990) suggested for the HPF. Our data from the fault zone (Figure 3b) strongly indicate dip-slip movement, for both the CE 1303 event and the longer-term behavior of the fault (section 4).

5.2.2. Slip Parameters of the CE 1303 Event

In our study, the dislocation of paleosol U6 in Trench Tc01 is 7.0 m, consistent with the geomorphic fault scarp, so the Holocene slip of 7.0 m at Trench Tc01 (section 4.2) can be related to the two events recorded at this site since the mid-Holocene (see supporting information). Assuming similar magnitudes and slip during each major earthquake, the slip was ~3.5 m during the CE 1303 event. Deng and Xu (1994) reported coseismic vertical displacements of ~3.5–5.0 m, in agreement with our measurements from Tc01. Smaller scarps and offsets have been recorded in this study, in the range of 2 m (Figures 5 and 6), and in agreement with results from Deng and Xu (1994) in the range of 0.7–2.4 m at the south end of the HPF. Late Pleistocene slip of 10.0 m at Trench Tc04 (Figures 6d and 12b) can be related to more than two events since the late Pleistocene.

The vertical slip rate can be estimated by using results from trenches Tc01 and Tc04. We take the age range of 4,550–6,790 year BP for U6 in trench Tc01 as the formation age (Figure 8) (Li, Mo, et al., 2014) and estimate the average vertical slip rate of the HPF to be ~1–1.5 mm/year during the past 7,000 year, equivalent to a horizontal extension rate of ~0.6–0.9 mm/year, assuming a fault dip of ~60°. We also interpret the age range of ~40–42 k BP for the formation age of gravel units of U14 and U17 in trench Tc04 (Figure 12b). This gives an average vertical slip rate of the HPF of ~0.24 mm/year during the late Pleistocene, equivalent to a horizontal extension rate of ~0.14 mm/year. Our Holocene result is comparable to the GPS-derived extension rate of 0.5–1.0 mm/year (Middleton et al., 2017; Wang et al., 2001; Zhang et al., 2003; Zhao et al., 2017), but the

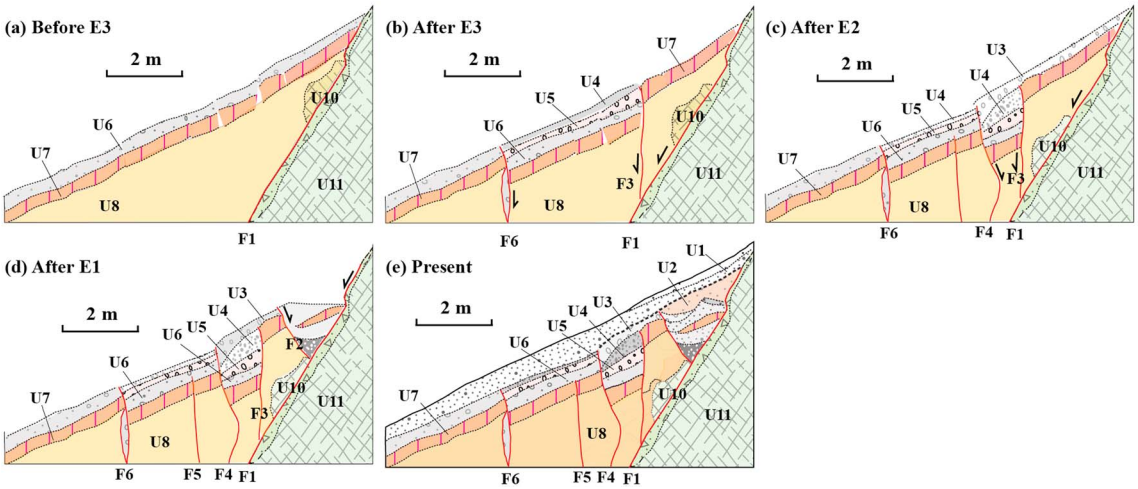

Figure 15. Schematic time sequence diagram of the three earthquake events identified in Trench Tc05.

Table 4
Fault Parameters of the HPF and Magnitude Estimates of CE 1303 Hongdong Earthquake

Parameter	Best estimate
Fault parameters	
Fault length (km)	98
Maximum throw (m)	5.0[b]
Maximum slip (m)	5.66
Representative throw (m)	3.5
Representative slip (m)	3.55
Magnitude estimates	
M_w from fault length[a]	7.5
M_w from maximum slip[a]	7.2
M_w from representative slip[a]	7.1
M_w from moment magnitude	7.5–7.6

[a]Scaling relationship from Wells and Coppersmith (1994). [b]Maximum vertical throw from Deng and Xu (1994).

average late Pleistocene rate is smaller than GPS-derived results. The slip rate is comparable to the other major active faults and grabens around the Ordos; see Middleton et al. (2017).

5.3. Magnitude of the CE 1303 Earthquake

We estimate a magnitude range for the CE 1303 Hongdong earthquake based on the results of this study (Table 4). The total length of the CE 1303 earthquake surface rupture zone is 98 km (see section 4.1 and Figure 7). The maximum throw during the event is 5.0 m (Deng & Xu, 1994). Using the representative surface dip of 62° (Figure 2d) and noting that motion is essentially dip slip, the maximum slip on the fault plane at the surface is 5.7 m. Applying scaling relationships between moment magnitude and fault length, representative, and maximum slip, we obtain values of M_w 7.5, 7.1 and M_w 7.2, respectively (Wells & Coppersmith, 1994) (Table 4). We also use the relationship of $M_w = 2/3 \log_{10}(M_o) - 6$ (Betbeder-Matibet, 2010; Hanks & Kanamori, 1979) to get another magnitude estimate, using a value for the seismogenic thickness of 20–25 km (Cai et al., 2014) and an representative fault dip of 62°. This calculation produces a value of M_w 7.5–7.6. Our results suggest that the previously estimated magnitude of M 8 (Meng et al., 1985; State Seismological Bureau (SSB), 1988; Xu & Deng, 1990; Yao et al., 1984) is an overestimate of the size of the CE 1303 earthquake. These previous estimates were derived from the intensity of shaking and the high death toll, rather than direct measurements of the rupture (length, slip). There is an important implication of the result for seismic risk assessment, as it means that earthquakes in the $M \sim 7$ range can cause serious death tolls in the Shanxi Graben and elsewhere around the Ordos.

In addition, the reduced magnitude estimate also shows a possible increased frequency of major earthquakes (Middleton et al., 2016). A shorter representative recurrence interval is required to accommodate a given strain rate across the HPF, with $M_w \sim 7.6$ events rather than M_w 8 events.

There is a wider application of this result. The CE 1556 Huaxian earthquake at the south side of the Ordos Plateau was the deadliest ever recorded (up to 830,000 deaths reported, e.g., Du et al., 2017) and has been widely interpreted to be an M 8 event (Shanxi Province Institute of Earthquake Engineering Investigation (SPIEEI), 2009; Zhang et al., 1998). Our study suggests that the Huaxian event also needs reevaluation. Given that the CE 1739 Yinchuan earthquake is now estimated to be in the M 7.1–7.6 range (Middleton et al., 2016), it is emerging that the great Ordos earthquakes are not exceptions to the global pattern that normal faults in the continents have upper magnitude limits of $M < 8$, where the magnitude is constrained through direct observations of the slip, rather than inferences based on shaking intensity and the number of casualties. A simple explanation for this limit lies in the relative steepness of normal faults: for a given seismogenic thickness, a normal fault dip-slip rupture reaches the full limit of the seismogenic layer at a smaller distance than a thrust, thereby limiting the maximum size of the earthquake (Figure 16). Strike-slip faults are not so constrained, because of their lateral propagation.

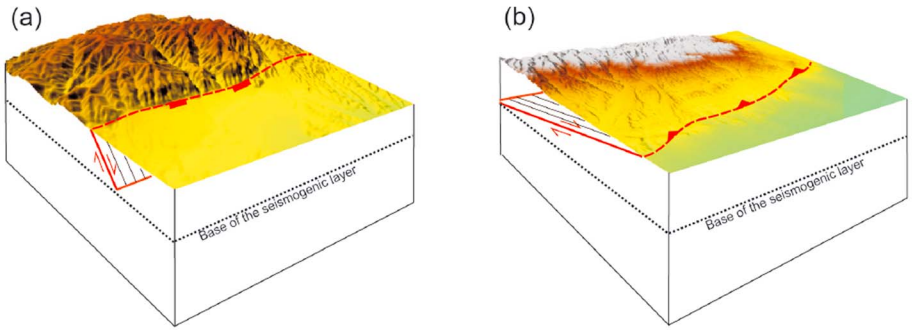

Figure 16. Schematic illustrations of (a) steeply dipping normal fault and (b) gently dipping thrust fault with same seismogenic thickness, showing the significant difference in fault area and hence maximum possible earthquake magnitude, if the whole seismogenic layer is ruptured.

Magnitude ~8 estimates for great Ordos earthquakes, including the Hongdong event, have previously been used to calculate the seismic moment release on faults in the region (Wang et al., 2011). It has been concluded that the west and eastern Ordos regions have a moment release surplus; that is, the historical earthquake record exceeds what is expected from the rates of moment accumulation, based on the GPS-derived velocity field. Our revised magnitude estimate for the Hongdong event suggests that the rates of accumulation and release are closer than previously thought (Wang et al., 2011), meaning that another (*M* 7) earthquake may occur sooner than if an *M* 8 event was expected.

6. Conclusions

Five trench excavations were conducted at four sites on the southern segment of the HPF. It is confirmed that the HPF has produced three major earthquakes during the Holocene and one event most likely in the late Pleistocene. Based on 31 AMS-^{14}C radiocarbon dating ages, the earthquakes are constrained to occur in age ranges CE 1,360–890 (1060–590 year BP), 3,310–3,210 year BP, <5,380 year BP, and <26,380 year BP. Therefore, a recurrence interval between 2,000 and 3,000 years is estimated during the last ~7,000 years. The latest event recorded in the trenches was the CE 1303 Hongdong earthquake.

The CE 1303 Hongdong earthquake occurred on the HPF and does not appear to have ruptured faults further north or south. Rupture length was ~98 km and representative slip 3.55 m, maximum slip 5.7 m, yielding a magnitude in the range M_w 7.1 to M_w 7.6 (Table 4). We estimate the average extension rate of the HPF to be 0.6–0.9 mm/year during the past 7,000 years, while late Pleistocene extension rate is lower, at 0.14 mm/year.

Our result shows that the CE 1303 event is not as large as the previously estimated magnitude 8.0. We need to use similar direct evidence to reevaluate other giant historical earthquakes around the Ordos Plateau, and not rely on historical records of shaking and fatalities.

An $M \sim 7$ magnitude for the Hongdong event is consistent with the recent reevaluation of the 1739 Yinchuan earthquake (Middleton et al., 2016), also previously regarded as an $M \sim 8$ event. These Ordos earthquakes are not exceptions to the global pattern of normal faults having $M < 8$ events, in contrast to both thrusts and strike-slip faults on the continents. A reasonable explanation lies in the relative steepness of such faults, in contrast to dip-slip thrusts, which reduces the seismogenic area for a given seismogenic thickness of the crust (Figure 16).

Acknowledgments

The KML file of our rupture map is available on request. SRTM is a product of NASA. All AMS-^{14}C ages in this paper were obtained by Beta Analytic Inc., USA. This research was jointly supported by the National Natural Science Foundation of China (grant 41502204), the Fundamental Scientific Research Fund in the IES, CEA (grant 2016IES0401, 2017IES0101), the Shanxi CBM United Fund (grant 2015012015), and the China Earthquake Administration Research Fund (grant 200908001). We are grateful to Yongkang Ran and Zihong Li at the China Earthquake Administration (CEA) for their assistance with fieldwork and J. Imber at the University of Durham for helpful discussions. Yueren Xu was sponsored as an Academic Visiting Scholar to University of Durham in UK by the China Scholarship Council (grant 201604190021).

References

Betbeder-Matibet, J. (2010). *Seismic engineering* (pp. 59–60). John Wiley & Sons.

Bi, L. S., He, H. L., Xu, Y. R., Wei, Z. Y., & Shi, F. (2011). The extraction of knickpoint series based on the high resolution DEM data and the identification of paleo-earthquake series—A case study of the Huoshan Mts. Piedmont fault (in Chinese). *Seismology and Geology*, *33*, 963–977.

Cai, Y., Wu, J. P., Fang, L. H., Wang, W. L., & Huang, J. (2014). Relocation of the earthquakes in the eastern margin of Ordos block and their tectonic implication in the transition zones of extensional basin (in Chinese). *Chinese Journal of Geophysics*, *57*(4), 1079–1090. https://doi.org/10.6038/cjg20140406

Chang, L. J., Wang, C. Y., & Ding, Z. F. (2011). Upper mantle anisotropy in the Ordos Block and its margins (in Chinese). *Science China Earth Sciences*, *54*, 888–900. https://doi.org/10.1007/s11430-4137-2

Deng, Q. D., Cheng, S. P., Min, W., Yang, G. Z., & Ren, D. W. (1999). Discussion on Cenozoic tectonics and dynamics of Ordos Block (in Chinese). *Journal of Geomechanics*, *5*, 13–21.

Deng, Q. D., Wang, K. L., & Wang, Y. P. (1973). On the tendency of seismicity and the geological set up of the seismic belt of Shanxi Graben (in Chinese). *Scientia Geologica Sinica*, *1*, 37–47.

Deng, Q. D., & Xu, X. W. (1994). Studies on the surface rupture zone of 1303 Hongdong earthquake of M=8 and paleoearthquakes of Huoshan Fault in Shanxi Province (in Chinese). *Earthquake Research in China*, *8*, 231–245.

Du, J. J., Li, D. P., Wang, Y. F., & Ma, Y. S. (2017). Late Quaternary activity of the Huashan Piedmont Fault and associated hazards in the southeastern Weihe graben, Central China. *Acta Geologica Sinica*, *91*(1), 76–92. https://doi.org/10.1111/1755-6724.13064

Geophysical Institute of Academy of Science of China (GIASC), & Macroseismic Survey Group of Seismologcial Team of Shanxi Province, China (MSGSTSPC) (2003). Survey report on September 17, 1303 Hongzhaoxian, Shanxi, earthquake (in Chinese). *Earthquake Research in Shanxi*, *114*, 23–30.

Hanks, T. C., & Kanamori, H. (1979). A moment magnitude scale. *Journal of Geophysical Research*, *84*(B5), 2348–2350. https://doi.org/10.1029/JB084iB05p02348

Hu, X. M., Wang, L. L., Zhe, J., & Lu, H. L. (2010). Morpho-sedimentary evidence of the Huoshan Fault's late Cenozoic right-lateral movement in the Linfen Graben, Shanxi Graben System, North China. *Frontiers of Earth Science in China*, *4*(3), 311–319. https://doi.org/10.1007/s11707-010-0110-9

Jiang, W. L., Xie, X. S., Wang, R., Wang, H. Z., & Feng, X. Y. (2004). Preliminary study on activity of Holocene paleoearthquakes along the Jiaocheng fault in the Shanxi down faulted system (in Chinese). *Journal of Seismological Research*, *27*, 184–190.

Jing, Z. J., Liu, F. X., Du, Y., & Xie, F. R. (2016). The activity characteristics of the southern section of the Taigu fault in Shanxi since the late Pleistocene (in Chinese). *Geological Bulletin of China*, *35*, 1559–1569.
Li, T. Y., Mo, D. W., Kidder, T., Zhang, Y. F., Wang, H. B., & Wu, Y. Q. (2014). Holocene environmental change and its influence on the prehistoric culture evolution and the formation of the Taosi site in Linfen basin, Shanxi province, China. *Quaternary International*, *34*, 402–408.
Li, Y. L., Yang, J. C., Xia, Z. K., & Mo, D. (1998). Tectonic geomorphology in the Shanxi Graben System, northern China. *Geomorphology*, *23*(1), 77–89. https://doi.org/10.1016/S0169-555X(97)00092-5
Li, Z. H., Liu, B. J., Yuan, H. K., Feng, S. Y., Chen, W., Li, W., & Kou, K. P. (2014). Fine crustal structure and tectonics of Linfen Basin from the results of seismic reflection profile (in Chinese). *Chinese Journal of Geophysics*, *57*, 1487–1497. https://doi.org/10.6038/cjg20140513
Liu-Zeng, J., Klinger, Y., Xu, X. W., Lasserre, C., Chen, G. H., Chen, W. B., et al. (2007). Millennial recurrence of large earthquakes on the Haiyuan Fault near Songshan, Gansu Province, China. *B.S.S.A.*, *97*(1B), 14–34. https://doi.org/10.1785/0120050118
Ma, Z. J. (Ed.) (1993). *Research on earthquake and systematic hazard reducing in Linfen city, Shanxi Province* (in Chinese) (pp. 136–158). Beijing: Seismological Press.
McCalpin, J. P. (2009). *Paleoseismology* (pp. 1–153). San Diego, CA: Academic Press.
Meghraoui, M., Delouis, B., Ferry, M., Giardini, D., Huggenberger, P., Spottke, I., & Granet, M. (2001). Active normal faulting in the upper Rhine Graben and paleoseismic identification of the 1536 Basel earthquake. *Science*, *293*(5537), 2070–2073. https://doi.org/10.1126/science.1010618
Meng, F. X., & Lin, H. W. (1972). A brief introduction on studying of two strong earthquakes in Shanxi Province using ancient architectures and appendices (in Chinese). *Cultural Relics*, *4*, 5–22.
Meng, X. L., Yu, S. E., & Xi, Y. (1985). The investigations of deformation traces of Ms=8.0 earthquake in Hongdong, Shanxi Province (in Chinese). *Seismology and Geology*, *7*, 1–10.
Middleton, T. A., Elliott, J. R., Rhodes, E. J., Sherlock, S., Walker, R. T., Wang, W. T., et al. (2017). Extension rates across the northern Shanxi Grabens, China, from Quaternary geology, seismicity and geodesy. *Geophysical Journal International*, *209*, 535–558. https://doi.org/10.1093/gji/ggx031
Middleton, T. A., Walker, R. T., Parsons, B., Lei, Q., Zhou, Y., & Ren, Z. (2016). A major, intraplate, normal-faulting earthquake: The 1739 Yinchuan event in northern China. *Journal of Geophysical Research: Solid Earth*, *121*, 293–320. https://doi.org/10.1002/2015JB012355
Peltzer, G., Tapponnier, P., Zhang, Z. T., & Xu, Z. Q. (1985). Neogene and Quaternary faulting in and along the Qinling Shan. *Nature*, *317*(6037), 500–505. https://doi.org/10.1038/317500a0
Qi, S. Q. (1983). Research on some problems of M8.0 earthquake in Shanxi Province (in Chinese). *North China Earthquake Science*, *1*, 36–44.
Qi, S. Q. (2005). Some problems on strong earthquake with M 8.0 in 1303, Shanxi, China (in Chinese). *Earthquake Research in China*, *21*, 224–234.
Ran, Y. K., Chen, L. C., Chen, J., Wang, H., Chen, G. H., Yin, J. H., et al. (2010). Paleoseismic evidence and repeat time of large earthquakes at three sites along the Longmenshan fault zone. *Tectonophysics*, *491*(1-4), 141–153. https://doi.org/10.1016/j.tecton.2010.01.009
Reimer, P. J., Baillie, M. G. L., Bard, E., Bayliss, A., Beck, J. W., Bertrand, C. J. H., et al. (2004). IntCal04 terrestrial radiocarbon age calibration, 0–26 calkyr BP. *Radiocarbon*, *46*(03), 1029–1058. https://doi.org/10.1017/S0033822200032999
Ren, J. Y., Tamaki, K., Li, S., & Zhang, J. (2002). Late Mesozoic and Cenozoic rifting and its dynamic setting in Eastern China and adjacent area. *Tectonophysics*, *344*(3-4), 175–205. https://doi.org/10.1016/S0040-1951(01)00271-2
Shanxi Province Institute of Earthquake Engineering Investigation (SPIEEI) (2009). *Atlas of Shanxi earthquake isoseismal* (in Chinese) (pp. 1–72). Beijing: Seismological Press.
Shanxi Provincial Geological Exploration Bureau (SPGEB) (1975). Scale of 1:200,000 Geological Map of Huozhou.
Shen, Z. K., Wang, Y. G., Gan, W. J., Li, T. M., & Zeng, Y. H. (2004). Crustal stress evolution of the last 700 years in North China and earthquake occurrence (in Chinese). *Earthquake Research in China*, *20*, 211–228.
Sieh, K., Stuiver, M., & Brillinger, D. (1989). A more precise chronology of earthquakes produced by the San Andreas Fault in South California. *Journal of Geophysical Research*, *94*(B1), 603–623. https://doi.org/10.1029/JB094iB01p00603
Sieh, K. E. (1978). Prehistoric large earthquakes produced by slip on the San Andreas fault at Pallett Creek, California. *Journal of Geophysical Research*, *83*(B8), 3907–3939. https://doi.org/10.1029/JB083iB08p03907
State Seismological Bureau (SSB) (1988). *Research on active faults system around the Ordos block* (in Chinese). Beijing: Seismological Press.
Sun, H. Y., He, H. L., Ikeda, Y., Kano, K., Shi, F., Gao, W., et al. (2015). Holocene paleoearthquake history on the Qingchuan fault in the northeastern segment of the Longmenshan Thrust Zone and its implications. *Tectonophysics*, *660*, 92–106. https://doi.org/10.1016/j.tecto.2015.08.022
Wang, H., Liu, M., Cao, J., Shen, X., & Zhang, G. (2011). Slip rates and seismic moment deficits on major active faults in mainland China. *Journal of Geophysical Research*, *116*, B02405. https://doi.org/10.1029/2010JB007821
Wang, N. L., Yang, J. C., Xia, Z. K., Mo, D. W., Li, Y. L., & Pan, M. (1996). *Cenozoic sedimentation and tectonic geomorphology of the Shanxi grabens* (in Chinese) (p. 400). Beijing: China Science Publishing Press.
Wang, Q., Zhang, P. Z., Freymueller, J. T., Bilham, R., Larson, K. M., Lai, X. A., et al. (2001). Present-day crustal deformation in China constrained by global positioning system measurements. *Science*, *294*(5542), 574–577. https://doi.org/10.1126/science.1063647
Wang, R. D. (2003). *Collection of earthquake monument in Shanxi Province* (in Chinese) (p. 673). Taiyuan: Beiyue Literature and Art Press.
Wells, D. L., & Coppersmith, K. J. (1994). New empirical relationships among magnitude, rupture length, rupture width, rupture area, and surface displacement. *Bulletin of the Seismological Society of America*, *84*, 974–1002.
Wesnousky, S. G., Jounes, L. M., Scholz, C. H., & Deng, Q. D. (1984). Historical seismicity and rates of crustal deformation along the margins of the Ordos block, north China. *Bulletin of the Seismological Society of America*, *74*, 1767–1783.
Working Group on Historical Earthquake Compilation of Shanxi Province Earthquake Administration (WGHECSPEA) (1991). *Compilation of historical earthquake literature in Shanxi Province* (in Chinese) (p. 476). Beijing: Seismological Publishing House.
Xie, X. S., Jiang, W. L., Wang, H. Z., & Feng, X. Y. (2004). Holocene activities of the Taigu fault zone, Shanxi Province, in relation to the 1303 Hongdong *M* = 8 earthquake (in Chinese). *Acta Seismologica Sinica*, *26*, 281–293.
Xu, J. H., Xie, X. S., & Sun, C. B. (2011). The Holocene active evidence on the Longci-Yukou segment of Luoyunshan frontal fault zone, Shanxi (in Chinese). *Seismology and Geology*, *33*, 855–864.
Xu, X. W., & Deng, Q. D. (1990). The features of late Quaternary activity of the piedmont fault of Mt. Huoshan, Shanxi Province and 1303 Hongdong earthquake (Ms=8) (in Chinese). *Seismology and Geology*, *12*, 21–30.
Xu, X. W., & Ma, X. Y. (1992). Geodynamics of the Shanxi rift system, China. *Tectonophysics*, *208*(1-3), 325–340. https://doi.org/10.1016/0040-1951(92)90353-8
Xu, X. W., Ma, X. Y., & Deng, Q. D. (1993). Neotectonic activity along the Shanxi rift system, China. *Tectonophysics*, *219*(4), 305–325. https://doi.org/10.1016/0040-1951(93)90180-R

Xu, Y. R. (2013). A Study on the Late Quaternary faulting of the Huoshan Piedmont Fault Zone in the central Shanxi faulted basin belt (in Chinese) (PhD thesis). Institute of Geology, China Earthquake Administration.

Xu, Y. R., He, H. L., Deng, Q. D., Wei, Z. Y., Bi, L. S., & Sun, H. Y. (2013). Quantitative river geomorphic parameters surrounding Mts. Huoshan, Shanxi Province and their tectonic implication (in Chinese). *Quaternary Sciences*, *33*, 746–759. https://doi.org/10.3969/j.issn.1001-7410.2013.04.12

Xu, Y. R., Shen, X. H., He, H. L., & Chen, L. Z. (2011). Application of CBERS-02B satellite images to Mt. Huoshan piedmont active fault mapping (1:50,000 scale) (in Chinese). *Science China: Information Sciences*, *41*, 202–212.

Yao, G. G., Jiang, Y., & Yu, X. M. (1984). Investigation on the 1303 Zhaocheng Shanxi, earthquake (M=8) and its parameters concerned (in Chinese). *Journal of Seismological Research*, *7*, 313–326.

Zhang, P. Z., & Gan, W. (2008). Combined model of rigid-block motion with continuous deformation: Patterns of present-day deformation in continental China. *Geological Society of America Special Papers*, *444*, 59–71.

Zhang, P. Z., Wang, M., Gan, W. J., & Deng, Q. D. (2003). Slip Rates along Major Active Faults from GPS Measurements and Constraints on Contemporary Continental Tectonics (in Chinese). *Earth Science Frontiers*, *10*, 81–92.

Zhang, Y. Q., Mercier, J. L., & Vergély, P. (1998). Extension in the graben systems around the Ordos (China), and its contribution to the extrusion tectonics of south China with respect to Gobi-Mongolia. *Tectonophysics*, *285*(1-2), 41–75. https://doi.org/10.1016/S0040-1951(97)00170-4

Zhao, B., Zhang, C. H., Wang, D. Z., Huang, Y., Tan, K., Du, R. L., & Liu, J. N. (2017). Contemporary kinematics of the Ordos block, North China and its adjacent rift systems constrained by dense GPS observations. *Journal of Asian Earth Sciences*, *135*, 257–267. https://doi.org/10.1016/j.jseaes.2016.12.045

Zhu, Z. P., Zhang, J. S., Zhang, C. K., Zhao, J. R., Liu, M. Q., Tang, Z. Q., et al. (1999). Study on the crust-mantle structure in the central and southern parts of Shanxi (in Chinese). *Acta Seismologica Sinica*, *21*, 42–49.